Available online at www.sciencedirect.com
SCIENCE DIRECT®
Journal of Nuclear Materials 349 (2006) 17–56
journal of nuclear materials
www.elsevier.com/locate/jnucmat

Thermodynamics of the O–U system. IV – Critical assessment of chemical potentials in the U–$UO_{2.01}$ composition range

Mehdi Baichi [a,1], Christian Chatillon [b,*], Gérard Ducros [a], Karine Froment [c]

[a] CEA Cadarache/DEN/DEC/S3C/LARA, Centre de Cadaranche, 13108 Saint Paul Lez Durance, France
[b] Laboratoire de Thermodynamique et Physico-Chimie Métallurgiques (UMR 5614, CNRS/UJF/INPG), E.N.S.E.E.G., BP.75, 38402 Saint Martin d'Hères, France
[c] CEA Grenoble/DTP/SE2T/LPTM, 17 rue des Martyrs, 38054 Grenoble cedex 9, France

Received 14 April 2005; accepted 2 September 2005

Abstract

A critical analysis of thermodynamic data available in the U–UO_2 system has been carried out with the twin aim of: (i) obtaining a reliable primary dataset for oxygen and uranium chemical potentials or partial Gibbs energies and, (ii) evaluating as realistically as possible the total uncertainties associated with these data. In order to perform this analysis, a array of regularly distributed values is built for sets of values, – ($\overline{G}_{O_2}$, O/U, T), – from which a direct comparison of different measurements can be undertaken within the evaluated uncertainty limits. The main conclusions of this analysis are (i) that major disagreements between different measurements are due to compositional uncertainties, (ii) and uncertainties associated with partial Gibbs energies are generally small except for those obtained by the isopiestic method of equilibrium with a given oxide. A set of selected data and proposed uncertainties is presented according to their distribution in our proposed array.

1. Introduction

For the analysis of the consequences of a severe nuclear accident, a knowledge of the thermodynamic properties of urania fuel, of the fission product elements and their compounds and of other materials, such as cladding and structural components is required. These properties are required to predict the chemical constitution of the mixture of the materials known as corium, at the appropriate high temperatures. The thermal hydraulic behaviour would depend on the chemical behaviour of the materials [1]. This paper deals with the critical analysis of the thermodynamic data of the U–UO_2 system, following a preceding one [2] on the phase diagram data for the same region. The aim of this critical analysis, – in conjunction with the two earlier analyses for the UO_2–UO_3 region [3,4], – is to build files of basic data for use in the optimisation of the thermodynamic data in conjunction with

* Corresponding author.
E-mail address: christian.chatillon@ltpcm.inpg.fr (C. Chatillon).
[1] Present address: IRSN, BP.17, 92260 Fontenay-aux-roses cedex, France.

0022-3115/$ - see front matter © 2005 Elsevier B.V. All rights reserved.
doi:10.1016/j.jnucmat.2005.09.001

phase diagram data with the PARROT software [5]. Indeed, producing a primary consistent data selection associated with a realistic evaluation of their associated uncertainties provide weightings for the individual data sets within the PARROT software. This step of the analysis is needed before any subsequent refinement by the optimization process. This process is dependent on the choice of thermodynamic model. For the production of very reliable thermodynamic descriptions, the two steps of the process must be carried out independently.

2. Thermodynamic data for the UO_2 stoichiometric compound

Formation enthalpy, entropy and heat capacities of UO_2 have been previously assessed by Rand et al. [6]. Among published data, these authors observed that the heat capacity of UO_2, assumed to be of stoichiometric composition, increases above ≈1800 K, and at 2670 K the measurements of enthalpy increments suggest a change of C_p^o behaviour, which becomes constant up to the melting temperature. The occurence of some kind of transition at 2670 K was at that time related to the prediction by Bredig [7] of a so-called λ transition in fluorite type crystals for $T \cong 0.8T_m$ (T_m: melting temperature). Bredig also proposed some variation of the transition temperature with the stoichiometric composition of the compound.

At that time and later, theoretical studies [8–21] provided estimates and fits to original C_p^o values on the basis of theoretical formulae taking account of different contributions to the heat capacity of UO_2: harmonic and anharmonic lattice vibrations, thermal expansion, defects or electronic contributions. Integration of C_p^o values were performed in order to recalculate the enthalpy increments at high temperature and to compare directly with calorimetric results. All these contributions never entirely reproduced the measured values of enthalpy at high temperature, showing that some additional contributions were present at $T > 2600$–2700 K.

These difficulties stimulated some further experimental work the aim of which was to try to measure directly the heat capacity in the high temperature range.

As already summarized by Hyland and Ohse [19], the direct calorimetric measurements of C_p^o were for relatively low temperature ranges, up to 1000 K, except the technique used by Affortit [22] and Affortit and Marcon [23]. Later Hiernaut and Ronchi [24], Hiernaut et al. [25], Ronchi et al. [26], Ronchi and Hyland [27], Halton et al. [28], and Ronchi and Hiernaut [29] used a laser pulse heating technique followed by cooling curve analysis for the solid and liquid UO_2. Neutron diffraction was used by Hutchings and coworkers [30–33] to examine the nature of the λ transition. The results of these high temperature measurements are presented in Table 1. Direct analyses of these measurements as well as their intercomparison is difficult and not very reliable owing to the numerous parameters that are required to perform and analyse these measurements, and moreover, assumptions or modelling are needed to obtain the pertinent parameters or required physical properties.

From neutron diffraction, coherent diffuse and inelastic scattering, Hutchings and coworkers [30,33] deduced that the Frenkel defect (3:1:2) is probably the main defect that sustains the λ transition. Affortit [22] and Affortit and Marcon [23] observed a clear and anormalous increase of C_p^o for $T > 1800$–2000 K, but not associated to a first order transition ($\Delta_t H > 0$) in the 2500–3100 K range, with hyperstoichiometric (2.004–2.1) UO_{2+x} samples. Hiernaut et al. [25] and Ronchi and Hiernaut [29] observed clearly a first order transition for UO_2 samples under a reducing atmosphere and consequently with a somewhat hypostoichiometric lattice. For oxidizing atmospheres, the first order transition disappears and these authors concluded that an evolution to a second order transition exists at the stoichiometric composition and for a critical temperature $T_c = 2670$ K. In the liquid phase these authors [26] observed first a sharp decrease of C_p^o from the solid value by more than 50% up to 4000 K, followed by a slight increase up to 8000 K.

In addition to the discussions presented by all the authors for the evaluation of the real uncertainty range, we propose to analyse their results in relation to the chemical behaviour of the UO_2 compound due to vaporization processes, which occur in this very high temperature range.

In the $UO_{2\pm x}$ solid phase, our first analysis of liquidus and solidus experiments which were performed near the melting point [2], showed that vaporization moves the sample composition toward the congruent one, UO_{2-x}, a feature already analyzed at lower temperature by mass spectrometry. Increasing the temperature would require that in order to avoid such changes of composition, either a closed vessel or a drastic reduction of the time for an experiment would be required.

Table 1
Experimental studies performed in the high temperature range ($T > 2500$ K) in view of determining the structural causes of heat capacity increase of the UO_2 compound

Authors (date) [Refs.]	Experimental technique	Temperature range (K)	Experimental conditions	Determined property and conclusions
Hutchings and coworkers [30–33]	• Neutron diffraction • Coherent diffuse and inelastic scattering	293–2930	• W encapsulation • Deterioration at $T > 2500$ K caused by evaporation (O/U decrease)	• Frenkel oxygen lattice disorder at $T > 2000$ K • Lattice expansion • Ionic potentials • Elastic stiffness constants
Affortit [22] Affortit and Marcon [23]	• Pulse Joule heating and heat balance against electrical energy (1/10 to 1 s/pulse) for a UO_2 wire (5 mm diameter)	1350–3150	• Thermocouples in situ • Best conditions obtained under vacuum conversely to Ar atm • Corrections for vaporisation • O/U > 2	• C_p^o direct determination • Important variations according to stoichiometry ($O/U = 2 \pm x$): $\delta C_p^o/C_p^o \sim 2$–3.6% for $\delta x = 0.01$ respectively at 2500 and 3000 K • C_p^o systematically lower than deduced from enthalpic increment in calorimetry
Hiernaut et al. [25]	• Laser pulse heating and thermal analysis of cooling curves for UO_2 solid sphere (0.05–0.15 s/pulse)	1500–3060	• Autoclave with high pressure (2–75 bars) • He or Ar + 3% H_2 • Sustained ball ($\leqslant$1 mm diameter) by four sonic waves on a W needle • Analysis as a function of shot's numbers	• Search for the λ transition • λ transition is occurring only for $O/U \leqslant 2$ • Evolution of T_λ which increases with hyperstoichiometry as revealed from different experimental pressures (see analysis in the text)
Ronchi et al. [26]	Ditto	3100–8000	Ditto	• C_p^o liquid
Ronchi and Hiernaut [29]	• Laser pulse on ThO_2	1500–4500	Ditto with pure Ar or O_2	• Observation of λ transition for O/Th = 2 or 1.98 • Proposition of T_λ evolution as a function of O/Th ratio • Same for UO_2 in relation with phase diagram

The first solution was satisfactorily employed with double walled tungsten cells for drop calorimetry; tungsten contamination of stoichiomeric UO_2 found to be negligible [34,35] and the evolution of UO_2 towards $UO_{1.98}$ limited and probably due to oxygen leaks by diffusion through the walls, as shown by Edwards et al. [36] in the very high temperature range of experiments. For these reasons, we do not raise questions or doubts about these calorimetric measurements, even if, as pointed out by Hyland and Ohse [19], the derived C_p^o values cannot give sufficiently good indications in the very high temperature region about the evolution of C_p^o with temperature in the liquid phase. Hutchings [30] observed some problems at $T > 2500$ K due to vaporization probably because the tungsten W welded containers allowed some vaporization processes to occur because of the free volume. Moreover, as pointed out in calorimetry, the UO_2 composition can become $UO_{1.98}$ due to oxygen leaks by diffusion through the walls, this change being in agreement with chemical forces that drive the system toward the congruent composition.

The second solution is the use of pulsed methods in order to avoid any significant vaporization phenomenon. Earlier, Christensen [37] observed that UO_2 heated at 2973 K in 20 s under 1 bar of He became $UO_{1.997\pm0.002}$. Decreasing the pulse time in the range 0.1–1 s, under vacuum, Affortit and Marcon [23] observed oxygen composition decreases less

than $\delta x = 0.005$ for relatively large UO_2 wires (4–5 mm diameter). Indeed, the Joule heating by an internal electrical pulse favours the temperature increase of the bulk material which effectively reduces the extent of vaporization at the surface. The authors observed that the use of a neutral atmosphere was not satisfactory due to convective effects. Hiernaut et al. [24,25] and Ronchi et al. [26] proposed the use of very high pressures to avoid any vaporization from the small UO_2 spheres (<1 mm diameter) used. In fact, as shown in Fig. 1 (built from table II in Ref. [25]), the temperature of the λ transition increases slightly in cumulative laser shots at constant pressure and clearly from high to lower pressures, and finally agrees with the transitions for the reducing conditions that were assumed by the authors with a gas mixture of 3% H_2 in Ar. These observations show clearly that the vaporization process exists that pulls the composition of the UO_2 sphere towards the congruent (or azeotropic) one. As we have calculated this composition from a thermodynamic optimisation of the U–O system [38,39], and according to our first analysis [2] of the intercept of the congruent line with the solidus as measured by Bates [40], we can postulate that the UO_2 spheres can only reach the $UO_{1.94}$ limiting composition (minimum hypostoichiometric composition, see Fig. 2) at ~ 3050 K, but never become richer with uranium when operating with solids. Thus, the evolution of the λ transition temperature as modelled by Ronchi and Hiernaut [29] should be first limited to this operating range to be consistent with their experimental capabilities and the congruent behaviour of UO_2. One more aspect to consider is the rate of exchange between the solid (or liquid) sample and the Knudsen layer of vapours that ultimately controls the diffusion of vapours into the high pressure buffer gas (chemical diffusion and thermal diffusion). On the basis of the Knudsen formula, for $p \cong 0.1$ bar at the melting temperature, the number of evaporated moles leaving the surface of a 1 mm sphere and entering into the Knudsen layer equals 9.4×10^{-5} mol s^{-1} or 2.5×10^{-2} g s^{-1}. These values compared to about 5.7×10^{-3} g for the sphere, indicates that the whole sample is rapidly affected by the enrichment of the Knudsen layer. It is probably for this reason that the laser heating under oxidizing conditions allows the UO_2 sample to stay quasi-stoichiometric or even hyperstoichiometric, but still only to a limited extend in relation to not necessarily the high pressure of the buffer gas but more surely to the oxygen content of the buffer gas that counteract the loss of oxygen by vaporisation of uranium oxides. In the absence of oxygen, the buffer gas does not efficiently prevent the occurrence of vaporization processes.

Concerning the liquid phase analysis of Ronchi et al. [26], the sudden decrease of the heat capacity C_p^o after melting is to be related to the displacement

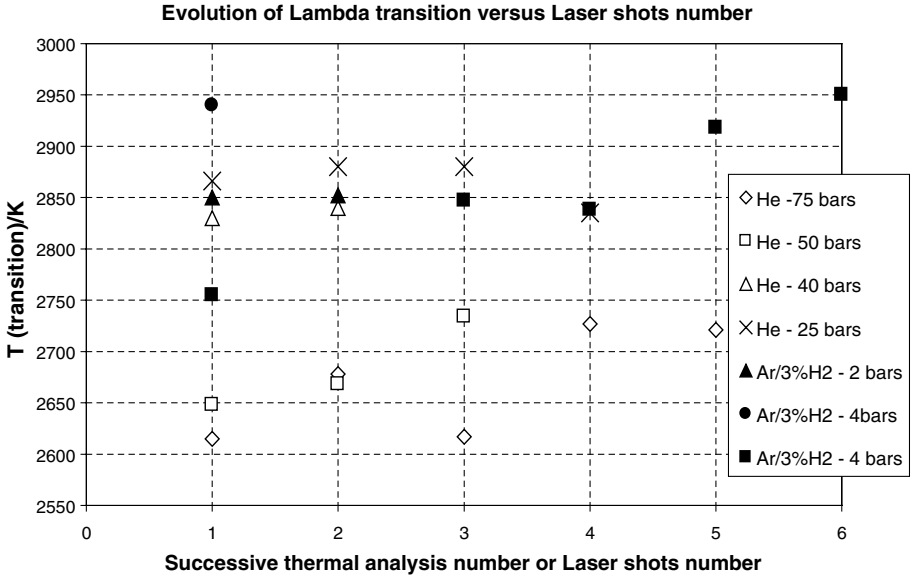

Fig. 1. Evolution of the observed temperature for the λ transition by thermal arrest decreasing temperature in the laser heating experiments of Hiernaut et al. [25] as a function of the shots number, run with different atmospheres compositions and total pressures.

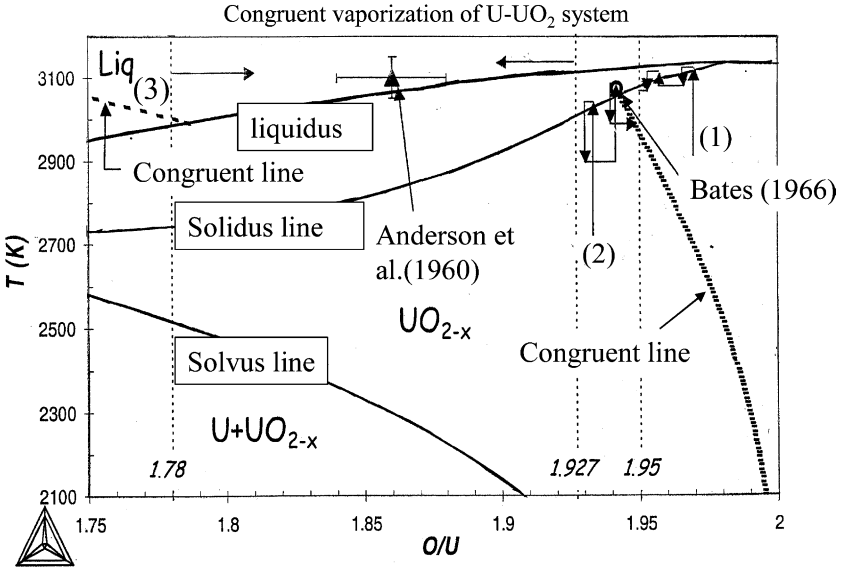

Fig. 2. Congruent vaporization composition lines as calculated by Baïchi et al. [38,39] for the UO_{2-x}(s) and liquid (U–O) phases. Any matter loss by vaporization drives the condensed initial composition of any samples chosen on every side of these lines towards these congruent composition lines. Bates [40] and Anderson et al. [41] compositions published as 'final and reproducible compositions' agreed with Baïchi et al. [2,38,39] thermodynamic calculations. In the solid UO_{2-x} phase, the O/U = 1.94 composition is the minimum one that can be reached by vaporisation losses when starting from UO_2 composition [40].

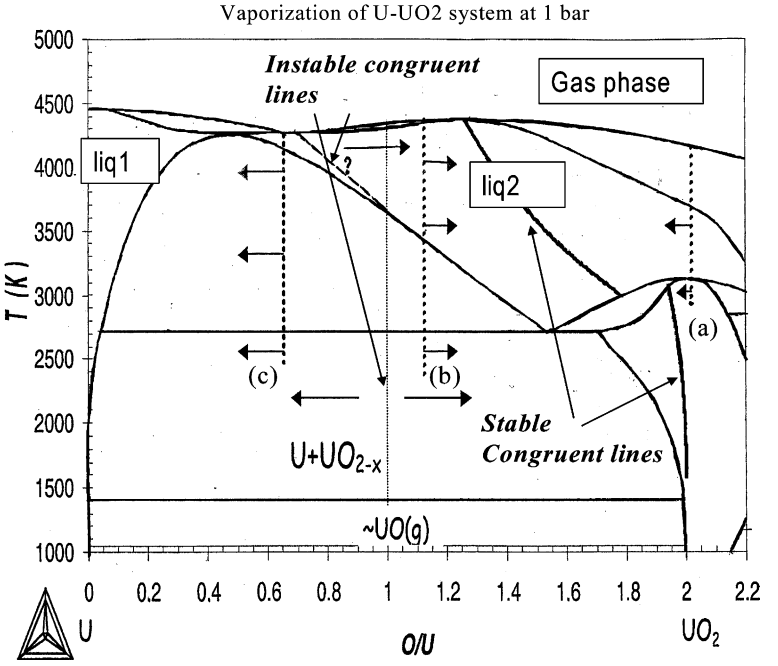

Fig. 3. Calculated congruent composition lines [2,38,39] for vaporization in the U–UO_2 system up to the gas phase at 1 bar. The liquid line as calculated shows a large deviation from the U/O = 2 stoichiometric composition. The arrows take account of the nature of the congruent state, stable or unstable, – in order to show the direction of composition evolutions for the condensed phases when matter loss occurs by vaporization.

of the congruent line towards richer compositions in uranium for the liquid phase as shown in Fig. 3 and measured in the liquid phase by Anderson et al. [41] (Fig. 2). Indeed, as temperature increases, the

chemical reactions also become faster as it is observed by the authors for the reaction with the W needle holder. Calculating the C_p^o value from melting to 4000 K for our congruent liquid line composition according to ideal law (Neumann-Kopp rule) from constant C_p^o for UO_2(l) (131 J K^{-1} mol^{-1}) deduced from drop calorimetry and U(l) [42], leads to a 9–18% decrease. The much larger decrease (about 50%) as measured by laser pulse technique is difficult to explain and is probably due to some unknown factor.

As a conclusion, we disagree with the recent analysis of Fink [21], who introduced results from the laser pulse technique into the analysis of the earlier conventional calorimetric measurements, and we prefer to retain Fink's first analysis [15] for the UO_2 stoichiometric compound:

- C_p^o fitted up to 2670 K according to formulae taking into account different contributions,
- C_p^o constant in the 2670–3128 K range,

$$C_p^o = 167.04 \text{ J mol}^{-1} \text{ K}^{-1} \quad (1)$$

from

$$H(T) - H(298.15) = 167.04T - 218\,342 \text{ J mol}^{-1}. \quad (2)$$

- Melting enthalpy as deduced from the two drop calorimetry measurements combined:

$$\Delta_m H^\circ = 75.8 \pm 2.3 \text{ kJ/mol} \quad (\text{at } T_m = 3128 \text{ K} \pm 15 \text{ K}) \quad (3)$$

as shown in Fig. 4 from drop calorimetry results of Hein et al. [43] and Leibowitz et al. [44,45].

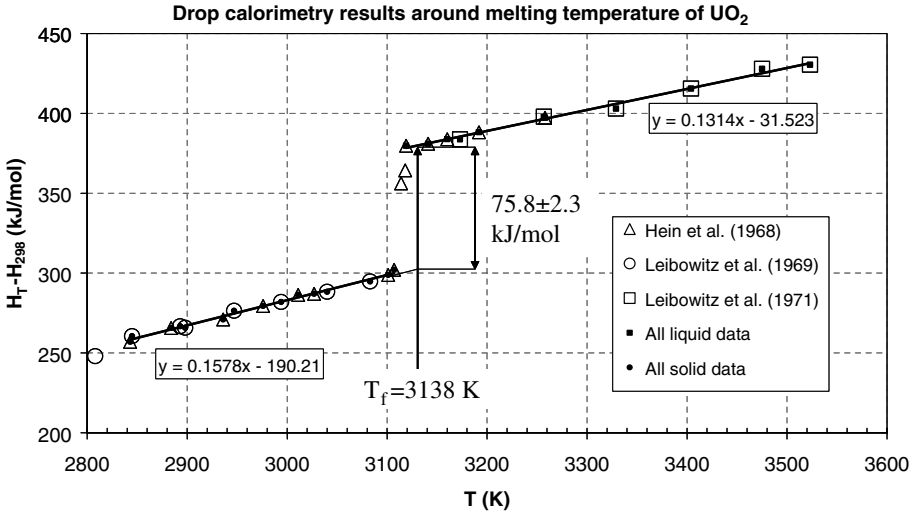

Fig. 4. Calculation of the melting enthalpy for UO_2 (s → l) from enthalpic increments as measured by drop calorimetry [43,35,44].

Table 2
Thermodynamic data for the stoichiometric UO_2 compound as retained in this work

Thermodynamic property	Value retained and uncertainty				References
$\Delta_f H^\circ$(298.15 K)	-1084.9 ± 0.8 kJ mol^{-1}				Rand et al. [6], Younés et al. [71]
S°_{298}	77.03 ± 0.20 J mol^{-1} K^{-1}				Rand et al. [6], Younés et al. [71]
C_p^o	$a + bT + cT^2 + dT^{-2}$ J mol^{-1} K^{-1}				Fit from Fink [15] selection
T range	**a**	**b**	**c**	**d**	
298–1300	75.39	1.1768×10^{-2}	-1.56227×10^{-6}	-1.34765×10^{6}	
1300–1800	241.229	-1.44922×10^{-1}	4.02834×10^{-5}	-5.6886×10^{7}	
1800–2300	1156.39	-7.93972×10^{-1}	1.69881×10^{-4}	-5.97222×10^{8}	
2300–2673.3	2251.53	−1.42985	2.73723×10^{-4}	-1.55975×10^{9}	
2673.3–3128	167.04				
T melting	3128 ± 15 K				Baïchi et al. [2]
$\Delta_m H$	75.8 ± 2.3 kJ mol^{-1}				This work from Hein et al. [43] and Leibowitz et al. [35,44]
C_p^o(liquid)	131.4 ± 4 J mol^{-1} K^{-1}				Rand et al. [6], this work

- $C_p^{\circ}(UO_2, l)$ is assumed to be constant according to drop calorimetry, that is

$$C_p^{\circ}(l) = 131 \pm 4 \text{ J mol}^{-1} \text{ K}^{-1} \quad (4)$$

as analysed by Hyland and Ohse [19] in case of constant C_p° and in agreement with the earlier proposition of Rand et al. [6]. Compared to our selection, the new and different values adopted by Fink in Ref. [21] for C_p° (liquid, T_m) and melting enthalpy, are derived from constraints due to the decreasing C_p° values in the UO_2 liquid phase when introducing the values of Ronchi et al. [26].

The λ transition is assumed to be a second order transition ($\Delta_t H_{\lambda} = 0$) for O/U = 2, according to Hiernaut et al. [25] and becomes a first order one for O/U < 2. Its impact will be treated when modelling the UO_{2-x} solid solution. Our thermodynamic data as retained for the stoichiometric UO_2 compound are presented in Table 2.

3. Chemical potentials analysis

Experimental determinations of the oxygen potential in the $UO_{2\pm x}$ non-stoichiometric range are very important for a complete thermodynamic description and modelling of the UO_2 phase, in conjunction with the knowledge of the oxygen potential at the phase boundaries. The composition range from U/O = 2.01 to the upper limit rich with oxygen has been analyzed earlier [3,4], for intermediate temperatures 800–1800 K, and for equilibria with U_4O_9(s) and U_3O_8(s). The present analysis deals with compiled chemical potential determinations from the literature presented in Table 3, and concerns mainly the high temperature and the hyposto-ichiometric region. We report also three studies, which were not analysed earlier [3], and consider compositions very close to the stoichiometric one.

The main principle of the following analysis is to build a {chemical potential/temperature T/composition x} array in order to compare the many studies since the original data never overlap directly. Indeed, due to their mode of measurements, isothermal or iso-concentration experiments are not necessarily run according to regular temperature or concentration intervals. The first aim in building the array is to redistribute the measured property, the chemical potential in this case, according to a set of regularly spaced steps in a (T, x) array so that the different data sets can be compared. The second aim may be to decrease the number of original data points, if required for the further optimization procedure [5], which we shall use to describe the thermodynamic properties of the U–O system. This second aim was not really used in this study since among the whole set of measurements we did not observe a great number of determinations focused in a narrow domain – and hence leading de facto to an important weighting factor for these data in the further optimisation – as it was the case for determinations in the hyperstoichiometric domain [3]. As already explained [3] the redistribution of original measured property along this {T, x} array is not carried out in order to decrease the uncertainty in the data set by any least square fit procedure and for this reason we keep practically the same data number and the original uncertainty as evaluated hereafter for each data set in the final retained values of the array. The original analysed uncertainties will be used as weightings within the optimization procedure. However, we have to keep in mind that the primary least square fits performed on original data sets to redistribute the data for the regularly spaced array improve necessarily and unwillingly the final array basic data set whatever are the retained uncertainties. This feature is one more reason to keep the original analysed uncertainties for each measured property or each variable T or x. In the following analysis, each original determination is separately analysed.

3.1. Determinations in the hyperstoichiometric composition close to UO_2

As quoted by Markin and Bones [53], classical e.m.f. cells UO_{2+x}/ZrO_2 electrolyte/Ni, NiO or Fe, FeO built in a single compartment and purged by purified Ar, performs well as long as the oxygen potential of UO_{2+x} remains higher than the reference electrode Ni/NiO, that is for UO_{2+x} richer in oxygen than $UO_{2.01}$. For measurements at lower oxygen potentials, close to stoichiometric UO_2, it seems that e.m.f. measurements are disturbed, perhaps by gas transport within the cell or by a leak of gas from the cell. For this reason, Markin and Bones [53] and later Baranov and Godin [54] built cells with two isolated and independent electrode compartments, the ZrO_2 or ThO_2 electrolyte becoming separating walls, each of them purged separately by Ar [53] or maintained in vacuum [54]. In the device of Baranov and Godin, oxygen can be pumped electrochemically into the evacuated compartment and served as an intermediate oxygen

Table 3
Chemical potential determinations mainly for oxygen – as compiled from literature and experimental techniques with their conditions for measurement

Authors (date) [Refs.]	Temperature range (K)	Composition range (O/U)	Experimental technique and conditions for measurements
Aitken et al. [45]	2473–2873 Pyrometry $T_{gradient} \leqslant 10$ K	• 1.87–1.94 • Gravimetry by oxidation in air at 1223 K to U_3O_8 • Reproducibility = ±0.003	• Heterogeneous equilibrium of UO_2 in a $H_2(+H_2O) + Ar$ flow or pure H_2 flow • Inlet H_2 bubbling in H_2O and hygrometer at the exit (always 100 ppm H_2O) • Cooling in pure Ar under 1273 K • W furnace, Ta or Re basket for UO_2 sample • Search for congruent vaporization composition under H_2 flow at 2673 K (H_2O = 100 ppm)
Alexander et al. [46]	2290–2720 2110–2560 Pyrometry	• 1.97 • 2.00 Polarography, Calcination with unknown T	• Transpiration method in $Ar + H_2 + H_2O$ and $H_2 + H_2O$ flow • W furnace • Condensed residue analysed for U transport and determination of UO_2(g) pressure • Weight gain of a magnesium perchlorate tube (H_2O quantity ± 5%) in relation with the total gas volume flowed • The magnesium perchlorate is by-passed for transient regimes
Markin et al. [47]	2200–2400 Thermocouple for the reference Oxide, Pyrometry for UO_2 (±10 K)	• 1.917–1.989 • Metallography • CO reduction at 1123 K of UO_2 slightly oxidized by O_2 (known amount) • O_2 and CO_2 volumetry	• Isopiestic equilibrium with Cr/Cr_2O_3 and Nb/NbO at lower temperatures • In 15 mbar H_2 to favour gas exchange via H_2O/H_2 • Thermal diffusion between H_2 and H_2O checked and assumed to be negligible • W or Mo crucibles • Sealed vessel
Tetenbaum and Hunt [48]	2080–2705 K Pyrometry	• 1.87–2.00 • Gravimetry (T?)	• Transpiration method in H_2/H_2O gas flow • W reactor • Analysis of the residue of condensation (not used for oxygen potential analysis) • Quenching of the experiment with Ar flow • H_2O/H_2 from cylinder H_2 units and mixture of flows
Szwarc and Latta [49]	• 2471–2917 • Pyrometry (±10 K) • Black body hole in W with T different from UO_2 by less than 25 K	• 1.88, 1.92, 1.94 • Air oxidation into U3O8 at 1173 K (δ(O/U) ± 0.003)	• Transpiration method in H_2 and H_2–Ar gas flows • H_2O is an impurity • W open tube as a reactor • Thermobalance for continuous weight loss measurements • Determination of total vapour pressure
Wheeler [50]	• 1800–2000 • Pyrometry (calibration on standard lamp) ±10 K • δT = ±10 K	• 1.98–2.00 • CO reduction after slight oxidation of UO_2, at 1125 K • O_2 and CO_2 volumetry	• Isothermal heterogeneous equilibrium of $UO_{2\pm x}$ with C (graphite) under CO gas, sealed in a vessel • Quenching after two hours • The graphite container is a Knudsen cell (C activity = 1) • CO Pressure is fixed when filling and temperature corrections are done for total CO pressure determination (previous calibration)

Wheeler and Jones [51]	1950 K	• 1.988–2.0025	• Heterogeneous equilibria: -(a) with C + CO(g) in sealed vessel, -(b) CO/CO_2 flow, -(c) H_2/H_2O flow, -(d) with $Cr\text{-}Cr_2O_3$ in a sealed vessel
	Pyrometry (calibration on standard lamp)±10 K	• CO reduction of UO_2 at 1123 K after slight oxidation by a known O_2 volume	• H_2/H_2O by bubbling H_2 in a temperature controlled unit (275–290 K)
		• O_2 and CO_2 volumetry	• Quenching after 8 h
		• Hydriding of UO_{2-x} samples into UH_3	
Javed [52]	1873–2173 K Thermocouple (W/Re)	• 1.96–2.00 • Gravimetry at 1123 K 1123 K is a 'critical' temperature (sic).	• Heterogeneous equilibrium with H_2/H_2O and H_2/H_2O/Ar flow • W crucible (also Mo or Ir), W furnace • Quenching in He • H_2O/H_2 mixture obtained through refrigeration unit
Markin and Bones [53]	928–1297 Thermocouple	• 2.0–2.01 • Coulometry	• E.m.f. with Ni/NiO reference • Vacuum closed cells with two different and isolated compartments to prevent oxygen transport by the gas phase and Ni/NiO degradation
		• Check by polarography H_2 at 1650 °C, or CO/CO_2 10/1 at 850 °C, $O/U \cong 2.0 \pm 0.00013$	• Experiments run in pure Ar with two different and separate streams
Baranov and Godin [54]	973–1273 Thermocouple	• 2.0–2.0039 • Coulometry • Check by polarography	• E.m.f. with Ni/NiO reference • Vacuum closed cells with isolated compartments • Experiments run with a compartment the oxygen-pressure of which is measured also by ref. To air
Thomas et al. [55], Gerdanian and Dodé [56]	1173–1423 Thermocouple (±2 K)	• 2.0025–2.0300 • Thermogravimetry with ref: pure H_2, $O/U = 2.0003$ at 900 °C and U_3O_8 under air [53]	• Thermogravimetry • Heterogeneous equilibrium CO/CO_2
		• Reproducibility $\sim 10^{-4}$	• Uncertainty from gas flow: $\delta p_{O_2}/p_{O_2} = 0.038$ (authors)
Becker [57]	1942 2109	• 1.985–2.05 • 1.955–2.0	• H_2/H_2O flow method
Ackermann et al. [58]	1822–2186 1600–2300	• Diphasic U/UO_2	• Mass spectrometric identification of vapour species UO(g), UO_2(g) and U(g) • Knudsen target collection • Activity of oxygen for the $U\text{–}UO_2$ diphasic domains
Pattoret [59], Pattoret et al. [60], Drowart et al. [61], Pattoret et al. [62]	2250	• 1.80–2.00	• Isothermal mass loss in a Knudsen cell mass spectrometric experiment (vapor pressures) and activity of U
	2053–2492	• 1.975/1.989/1.997	• Knudsen cell mass spectrometry at constant composition (or controlled one) (vapor pressures)
	Pyrometry	• Polarography before and after experiment	• Measurements of U(g), UO(g), UO_2(g) partial pressures • Use of twin cells for UO_2 activity determination in the $U\text{–}UO_{2-x}$ diphasic domain and for congruent composition • Use of the congruent composition as a cross-check for calibration of composition • Evaluation of oxygen loss by diffusion through W cell walls ($\delta O/U < 0.003$)

(*continued on next page*)

Table 3 (*continued*)

Authors (date) [Refs.]	Temperature range (K)	Composition range (O/U)	Experimental technique and conditions for measurements
Storms [63]	1667–2175 Pyrometry (special device with photomultiplier) (±2 K)	• Calcination into U_3O_8 at 950 °C, 2 h • Reproducibility: ±0.002	• Knudsen cell mass spectrometry • W cells pre-degased and pre-equilibrated with samples • UO^+ ions observed from photo effects or thermal shields revaporization • U(g) coming also from thermal shields that can interfer at low U activity • Determination of U activity either from U(g) or UO(g)
Baichi et al. [64]	2020–2230 Thermocouple (W/Re) (±10 K)	• Diphasic U–UO_{2-x} with O/U = 0.35, 0.45 and 0.5	• Multiple Knudsen cell method, with special collimation device to prevent from re-vaporized molecular flows • W cells (4 cells in the same Ta envelope) • Determination of UO_2 activity by direct and in situ reference to pure UO_2(s)

buffer potential which is measured by a Fe/FeO electrode.

Because the chemical potential of oxygen close to the UO_2 stoichiometric composition range varies very significantly with composition, the composition is obtained by 'in situ' coulometric titration from a reference composition. To avoid some diffusion limitations and long time equilibration, the UO_{2+x} samples were in the form of thin flakes.

Markin and Bones [53] used as a reference some composition close to the stoichiometry, that is UO_2 treated at 1650 °C in H_2 or UO_2 treated in $CO/CO_2 = 10/1$ mixtures at 850 °C. As the CO/CO_2 mixture would produce the lowest Gibbs energy of oxygen, the authors assumed this reference to be strictly UO_2, with an uncertainty of the order of $\delta x = \pm 0.00013$. The uncertainty is also supposed to be the accuracy of their coulometric titration, which is in agreement with some cross-check performed by polarographic analysis at $O/U = 2.01 \pm 0.0005$. The composition for UO_2 treated by H_2 as already discussed by Schaeffer et al. [65], has an uncertainty $\delta x = \pm 0.001$ and indeed brackets largely the UO_2 reference composition obtained with CO/CO_2 mixtures by Markin and Bones which appears to be more accurate. For this reason we retain $\delta x = \pm 0.00013$, the estimated uncertainty of the authors.

Baranov and Godin [54] used an initial sample with $O/U = 2.0039 \pm 0.0001$ and checked by polarography to be 2.0041 ± 0.0002. We believe that the 2.0039 initial value is chosen by the authors in agreement with coulometric titration in order to match the 'vertical' voltage variation as measured for the stoichiometric UO_2 composition. Nevertheless, the total uncertainty on composition is calculated here from the readings of the graph and from the reference composition:

$$\delta x = ((\pm 0.00018)^2 + (\pm 0.0002)^2)^{1/2} = \pm 0.00027. \quad (5)$$

For temperature, we evaluate the thermocouple uncertainty $\delta T = \pm 5$ K as in Ref. [3], but for Baranov and Godin work we have to add the uncertainty of the readings to this thermocouple uncertainty:

$$\delta T = ((5)^2 + (10)^2)^{1/2} = \pm 11 \text{ K}. \quad (6)$$

The uncertainty for the measured Gibbs energies of oxygen comes from the e.m.f. stability voltage ± 2 mV, or ±770 J, and for Baranov and Godin from readings, ±3000 J. As the total uncertainty remains lower than 1%, we have chosen to fix the

value arbitrarily at 1% to avoid any abnormal and unrealistic value as discussed earlier by Labroche et al. [3]. We choose the same value 1% and for the same reasons also for the e.m.f. studies of Markin and Bones . The Gibbs energy as determined in those two e.m.f. studies are corrected and referred to our choice for the assessed e.m.f. of the Ni/NiO and Fe/FeO electrodes [3].

When plotting the experimental values of these two studies, Markin and Bones and Baranov and Godin, as presented in Figs. 5 and 6, we observe that the partial Gibbs energies of oxygen are in very close agreement for the O/U = 2 (stoichiometric compound) within their total uncertainty ranges as analysed above both for the composition and for the Gibbs energy. Thus, the disagreement observed between these two works for O/U > 2 can be considered to be real, and should be analysed.

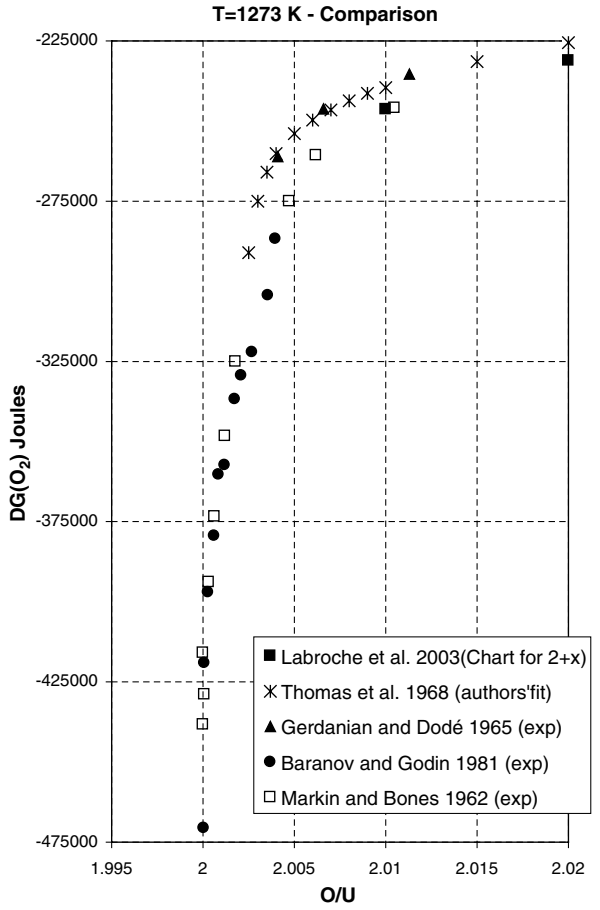

Fig. 5. Comparison of e.m.f. data from Markin and Bones [53] and Baranov and Godin [54] with TGA of Thomas et al. [55] for UO_{2+x} domain close to stoichiometry and the array values as retained in the preceding work by Labroche et al. [3] $T = 1273$ K.

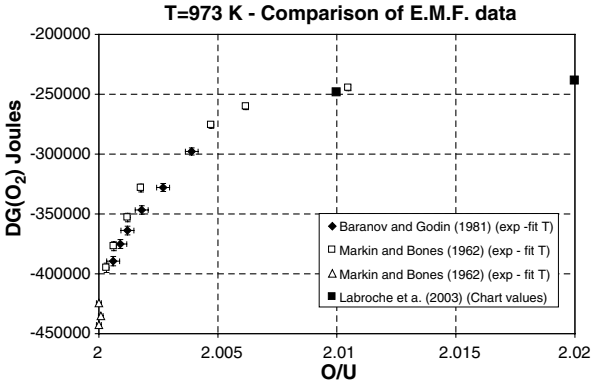

Fig. 6. Comparison of e.m.f. data from Markin and Bones [53] and Baranov and Godin [54] with the array values retained by Labroche et al. [3].

The mode of operating for the two e.m.f. works differs slightly. Markin and Bones start from UO_2 (reduced by $CO/CO_2 = 10/1$ at 850 °C), oxidize step by step the UO_2 flake in the Ar atmosphere by electrolysing through ZrO_2 the Ni/NiO electrode (coulometric titration) up to 2.01, and then reversibly reducing the UO_2 flake. Some runs were performed isothermally (973, 1123, 1273 K), others were performed for each composition step with variation of the temperature. By displaying the results of the isothermal runs and their intercept with least square fits of non-isothermal (fixed composition) runs, a perfect agreement is found, at least within our evaluated uncertainty range between these two sorts of independent runs, including those for which the composition is obtained electrochemically either by oxidation or by reduction.

Baranov and Godin [54] use a second and independent electrolyte on the other face of the UO_2 flake in order to reduce it by electrolysis. At the same time the oxygen pressure (or potential) of the UO_{2+x} sample was controlled by reference to the oxygen in the compartments of the cell, which could be adjusted by pumping this oxygen electrochemically through the ZrO_2 housing. The oxygen potential in thus adjusted using a combination of electrodes to the same value as the one continuously measured by the first electrolyte for UO_{2+x}. As there is no direct contact between the electrolyte in contact with the UO_2 flake and the electrolyte in contact with the Fe/FeO reference electrode, the oxygen chemical potential of the gas phase in the intermediate compartment is in fact an intermediate

oxygen potential for measuring the chemical potential of UO_{2+x}. The final measurement, by the first electrolyte is the oxygen potential of the gas phase in equilibrium with the UO_{2+x} flake and the gas phase potential is then known by the Fe/FeO electrode of the reference compartment. At each titration step, the e.m.f. voltage is measured as a function of temperature, and moreover one run was performed isothermally at 1273 K. The intercept of the non-isothermal runs with the only isothermal one at 1273 K shows consistent values. However, Baranov and Godin did not check the reproducibility of their measurements after reoxidizing the flake.

Internal consistency of these two sets of results, as well as their intercomparison are done by reporting their values on a single temperature-composition (T, x) array. Firstly, a least square fit $\overline{\Delta G_{O_2}} = f(1/T)$ for any constant composition (Fig. 7) allows us to build $\Delta G(O_2)$ versus T array from steps at 973, 1000, 1100, 1123, 1200, 1273 and 1300 K, including the temperature of the isothermal experiments. Then a second serie of regularly distributed values is obtained by fitting $\overline{\Delta G}(O_2)$ as a function of the composition, discarding the UO_2 reference or the closest compositions for which variations are too great and for each selected array temperatures the composition intervals are distributed according to O/U steps of 5×10^{-4} from O/U = 2.0005–2.01. For O/U values lower than 2.0005 an independent fit is made due to the sudden great variation of the Gibbs energy. Nevertheless, the redistribution of original data in this array never gives additional data, and is carried out within the experimental limits from each set of authors.

The resulting values of the array – with their original evaluated uncertainties – are then compared with direct isothermal runs as shown in Figs. 8 and 9. We report also in these figures the overlap with the preceding array as established by Labroche et al. [3] for UO_{2+x} with $2 + x \geqslant 2.01$. We observe that the connection is perfectly consistent for the Markin and Bones work. The results of the two e.m.f. studies analysed above disagree and more markedly at low temperatures. For the same Gibbs energy of oxygen, which is chosen as a reference due to the configurations of the cells and to their stability (±2 mV) – the difference observed for composition amounts to 0.00066. This difference is more than the sum of the two composition uncertainty ranges and the origin of these discrepancies can be discussed. Baranov and Godin invoked a possible disruption of the hermetic seals of the electrolyte cell around the UO_2 flake, which can explain the

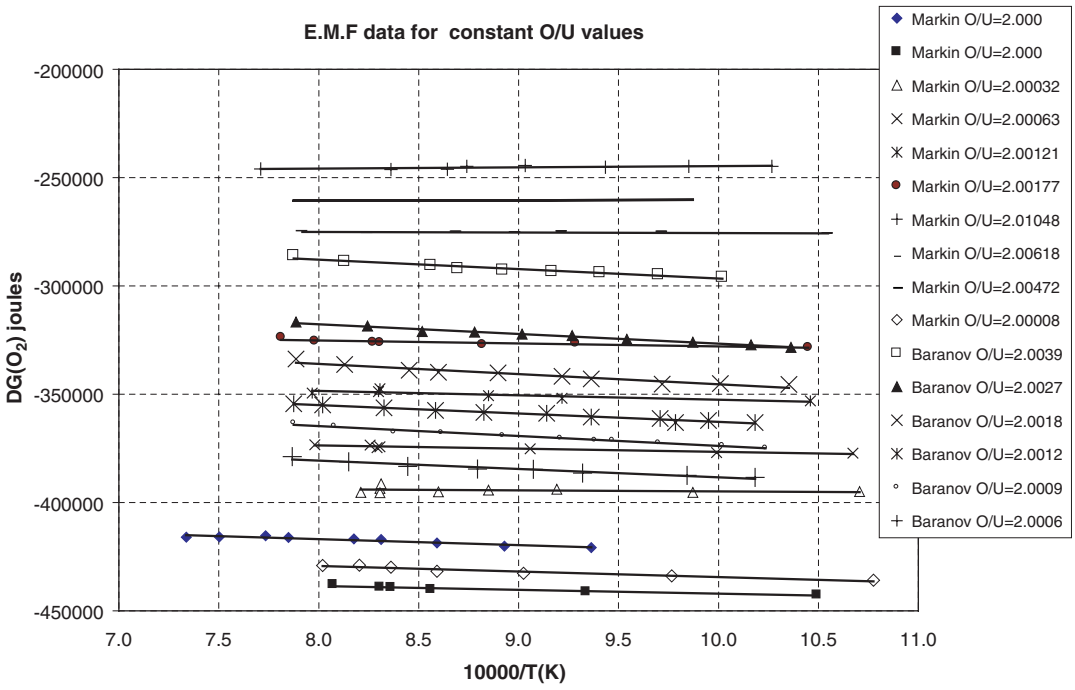

Fig. 7. Original e.m.f. data of Markin and Bones [53] and Baranov and Godin [54]. The fits versus temperature show a systematic trend in the slopes between these two groups: Baranov and Godin slopes are larger than those determined by Markin and Jones.

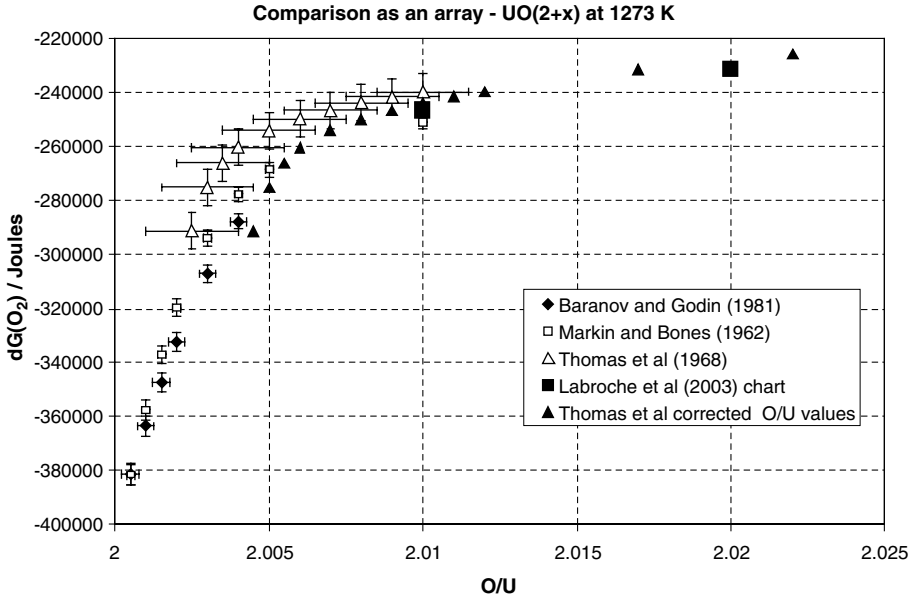

Fig. 8. Comparison of least square fitted values as stored in the array at 1273 K for each group of authors. We observe that – even shifted by $\delta x = +0.015$ for incomplete calcinations and nitrogen interaction – the Thomas et al. [55] values do not match correctly the Labroche et al. [3] array values, and moreover their general curvature remains more pronounced than those of Markin and Bones [53] or Baranov and Godin [54].

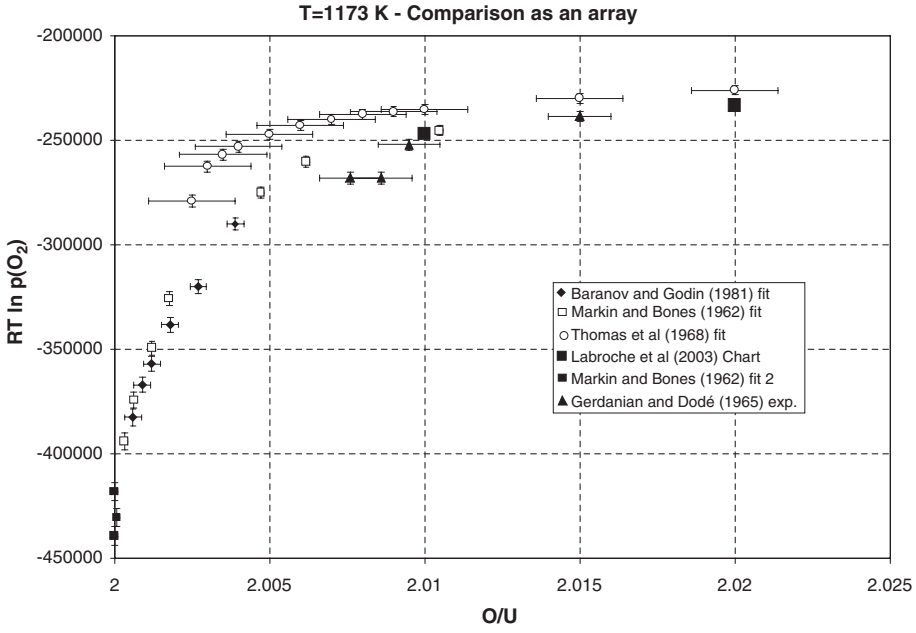

Fig. 9. Comparison of least square fitted values as stored in the array at 1173 K for each group of authors. Even shifted by $\delta x = +0.015$ for incomplete calcinations and nitrogen interaction the Thomas et al. [55] values cannot match correctly the Labroche et al. [3] array values, and moreover their general curvature remains more pronounced than those of Markin and Bones [53] or Baranov and Godin [54].

observed composition discrepancies, since recycled oxygen could increase the quantity measured by coulometric titration. This may explain samples richer in oxygen than Markin and Bones attributed to the same measured e.m.f. voltage, but we cannot explain why the isothermal run at 1273 K agrees

very well with the different runs performed at constant composition, except by some permeability of the Pt gaskets or electrolyte materials which would have to be reproducible for all the different experiments.

A second explanation of the difference between these two e.m.f. studies could be due to the structure of the cells, and especially in the case of Baranov and Godin, the measurement via the gas phase as an intermediate buffer phase may introduce some kinetic effects at the surface of the electrodes or the sample. The gas-surface reactions may be hindered as is known for free vaporisation of UO_2 [66] at high temperature, since there exists an evaporation coefficient α, evaluated as $\alpha \cong 1/3$ [59,60]. The same phenomenon was observed by Blackburn [67] with O_2(g) evaporating from U_3O_8 and U_4O_9. In case of such kinetic barrier at the UO_2/Pt/gas contact, the apparent chemical potential of oxygen would decrease by a quantity $RT\ln\alpha = -11\,670$ J at 1273 K which is on the order of the observed difference. Moreover, these evaporation coefficients follow an Arrhénius law, and generally α decreases with temperature, a feature which can explain the steeper slopes observed systematically by Baranov and Godin when compared to Markin and Bones in experiments performed at constant compositions (see Fig. 7).

Conversely, for measurements of Markin and Bones [53], the oxygen activity is directly measured from oxygen ions at electrodes, and this measurement avoids any conversion like $2O^-$ into O_2(g) or O^- into O(g) through a surface adsorption step which would require some activation energy.

Thermogravimetric measurements were performed by Gerdanian and Dodé [56] and Thomas et al. [55] under CO/CO_2 gas mixtures in the same composition range with some overlap in the 1173–1273 K temperature range. Labroche et al. [3] analysed the calcination method under air and deduced from the original work of Ackermann and Chang [68] under pure O_2 or $Ar + O_2$ mixtures that some influence of N_2 exists that explains the systematic trends observed between the studies of Gerdanian and Dodé and other studies for which calcinations were performed with pure oxygen or composition determined by other methods. For this reason the composition uncertainty (δx) is fixed to the same value as proposed in the Labroche et al. [3] study: $\delta x = \pm 1.5 \times 10^{-3}$, which is reasonably close to the reproducibility rather than to the absolute uncertainty. The uncertainty on the partial Gibbs energy proposed by the authors is $RT(\delta p_{O_2}/p_{O_2})$, (with $\delta p_{O_2}/p_{O_2} \cong \pm 0.038$), a value lower than 1%, and according to Labroche et al. [3], and as for the studies discussed above we attribute arbitrarily a minimum value of 1%. Thomas et al. propose in their Table 8 a fit of their values, which we use in our array and compare to Baranov and Godin [54] and Markin and Bones [53]; this comparison is shown in Fig. 8 for 1273 K. We observe that for all the works, displayed according to our array, there is some agreement within their uncertainty ranges, but Markin and Bones remain closer to Thomas et al., while those of Baranov and Godin only partialy overlap. We have to be aware, as already explained by Labroche et al. [3], that the calcinations at $T > 873$ K in fact do not produce U_3O_8 as stated by Thomas et al. [55] and Gerdanian and Dodé [56] but U_3O_{8-z}, the value of z increases with temperature (at 1173 K, O/U is 2.6512 rather than 2.6667). Consequently, values proposed by Thomas et al. and Gerdanian and Dodé should be shifted towards the stoichiometric composition. Thus, the overlap supports the values of Markin and Bones. As already stated by Labroche et al. [3] and observed in the U_4O_9–U_3O_8 composition range, we cannot retain the data of Thomas et al. and of Gerdanian and Dodé because the composition uncertainty cannot really be evaluated although the thermogravimetric studies were performed very carefully ($\delta T = \pm 2$ K, and $\delta G(O_2) < 1\%$). A comparison of the values of Thomas et al. at 1373 and 1423 K with the array of Labroche et al. [3] for $O/U = 2.01$ and 2.02 shows the same disagreement as for 1273 K that cannot allow, even with a simple and constant translation δx, the retention of these data: it is probable that a constant δx correction is not suitable to scale the results of these authors against the whole data set because of the influence of N_2 in the oxidation process.

As a conclusion, we retain the Markin and Bones [53] values, referred to our selected e.m.f. potential [3] because the measurements have been performed reversibly and the cell structure keeps a rather conventional direct means of operation. Moreover their results are within the trend essentially confirmed by Thomas et al. [55].

3.2. Heterogeneous equilibria methods and hypostoichiometric UO_{2-x}

These methods use a gas phase either the composition of which is known and its potential imposed

on the sample by flowing gas over it for a sufficient time to reach equilibrium or the role of which is to transport some of the components in order to equilibrate the $UO_{2\pm x}$ sample with a known mixture (Cr–Cr_2O_3 or Nb–NbO) the temperature of which is controlled and that operates at a cold point. These different studies are presented in Table 3 with their experimental conditions and the methods used to determine the $UO_{2\pm x}$ sample composition. Among the flow methods, Alexander et al. [46] and Tetenbaum and Hunt [48] used the transpiration method that ensures the accuracy of the pressure-flow relation because the arrangement of the hot zone of the reactor as well as the usual flow tests of the method avoid any reverse diffusion flow in the gas phase; appropriate apertures were present at the inlet and outlet of the reactor hot zone.

3.2.1. Calculation method and correction for reference

In transpiration [46,48], flow methods [45,52] and isothermal equilibration method [50] the authors give their reference equilibrium data as for instance

$$2H_2O(g) = 2H_2(g) + O_2(g) \quad (7)$$

and the Gibbs free energy in the form of a relation or referred to thermochemical tables or earlier compilations. In order to refer all these original data to the same reference, namely the JANAF tables 1998 [69], we compared the authors reference equilibrium Gibbs energy relations with those derived in the same temperature range from JANAF 1998, and we obtain the correction factors as presented in Table 4. The original published values of partial Gibbs energy of O_2 (in J) are also directly converted into partial Gibbs energy referred to the same standard state, the correction for 1 atm to 1 bar being included.

Although quoted in Table 3 as a determination according to the transpiration method, the Szwarc and Latta [49] work cannot be retained for different reasons:

- This flow method is run mainly to check constant vaporization rates, and consequently produces total vapour pressure as presented in their table III.
- The oxygen partial pressure is only deduced from H_2O impurities (their table I) and not clearly from a H_2O/H_2 controlled ratio.
- Their deduced $UO_2(g)$ vapour pressure is systematically higher than the UO(g) vapour pressure, in total contradiction with mass spectrometric results at lower temperatures and for the same composition, although the UO(g) species is observed in mass spectrometry to increase

Table 4
Correction factors in as published partial Gibbs energies of oxygen $\overline{\Delta G}_{O_2} = RT\ln p_{O_2}$ of authors heterogeneous equilibria data used to recalculate our partial Gibbs energy referred to JANAF 1998 tables [69]

Authors	$\overline{\Delta G}_{O_2}$ (J) $= RT\ln p_{O_2}$ referred to JANAF tables
Aitken et al. [45]	$\overline{\Delta G}_{O_2}$ (Aitken, Joules) $-11965.6 + 7.196T$, 2300 K $< T <$ 2800 K
Alexander et al. [46]	
Markin et al. [47]	• Cr/Cr_2O_3 at T_{ref}(1000–1200 K) and for $2200 < T < 2400$ K: $\overline{\Delta G}_{O_2} = \overline{\Delta G}_{O_2}$ (Markin, Joules) $-25108 - 560T/T_{ref} - 37.488T\log_{10}(T/T_{ref}) + 9.338T$ • Cr/Cr_2O_3 at T_{ref} (900–1200 K) and for $1600 < T < 1700$ K: $\overline{\Delta G}_{O_2} = \overline{\Delta G}_{O_2}$ (Markin, Joules) $-22402 - 560T/T_{ref} - 37.488\,T\log_{10}(T/T_{ref}) + 7.928T$ • Nb/NbO at T_{ref} (1200–1300 K) and for $T = 2200$ K: $\overline{\Delta G}_{O_2} = \overline{\Delta G}_{O_2}$ (Markin, Joules) $-25108 + 8835T/T_{ref} - 37.488T\log_{10}(T/T_{ref}) + 10.38T$ • Influence of thermal diffusion according to authors discussions: $H_2O(g)$ pressure may be decreased by a factor 4 and consequently $\overline{G}_{O_2}$ could increase $\sim 0.25RT = 3000$–5000 J, added to the above uncertainty
Tetenbaum and Hunt [48]	$RT\ln p_O$(ref. JANAF) $= RT\ln p_O$ (authors, Joules) $+ 5774.1 + 3.358T$ or $\overline{\Delta G}_{O_2} = 2RT\ln p_O$ (authors, Joules) $+ 523431.2 - 127.647T$
Wheeler [50]	$\overline{\Delta G}_{O_2} = \overline{\Delta G}_{O_2}$ (authors, Joules) $+ 903 - 0.56T$
Wheeler and Jones [51]	H2/H2O flow (1950 K) $\overline{\Delta G}_{O_2} = \overline{\Delta G}_{O_2}$ (authors, Joules) $-24235.4 + 134.626\,T - 37.489T\log_{10}T$ C/CO/UO_2 (same as in 1971 work [50]) CO/CO_2 flow (1950 K): $\overline{\Delta G}_{O_2} = \overline{\Delta G}_{O_2}$ (authors, Joules) $+ 8980.4 - 5.796T$ Cr/Cr_2O_3 same reasoning as for Markin et al. [44] at $T = 1950$ K: $\overline{\Delta G}_{O_2} = \overline{\Delta G}_{O_2}$ (authors, Joules) $-23868 - 560T/T_{ref} - 37.488\,T\log_{10}\,T/T_{ref} + 8.748T$
Javed [52]	$\overline{\Delta G}_{O_2} = \overline{\Delta G}_{O_2}$ (authors, Joules) $-24235.4 + 134.626T - 37.489T\log_{10}T$

relative to UO_2(g) with temperature. Further, use of the calcination method into U_3O_8 at 1173 K introduces a composition uncertainty of the order of $\delta x = -0.020$. All these reasons explain why the data of Szwarc and Latta [49] clearly differ from those of other studies.

For the equilibration with Cr/Cr_2O_3 or Nb/NbO [47,51] in a sealed quartz vessel initially filled with about 15 mbar of H_2, the authors showed that the two main gaseous species are H_2 and H_2O, meanwhile O_2 has a very low pressure. Consequently, their main assumption is that the H_2O/H_2 ratio in equilibrium with the reference mixture Cr/Cr_2O_3 (or Nb/NbO) at the cold point has the same value at the UO_2 sample surface; the gaseous equilibrium is achieved for the two species. Thus the authors have neglected thermal diffusion that favours accumulation of the lighter molecule, H_2 at the hot side (sample) and consequently decreases the H_2O pressure at the UO_2 sample surface. At the cold point $T = T_{ref}$:

$$4/3\mathrm{Cr(s)} + \mathrm{O_2(g)}\Delta 2/3\mathrm{Cr_2O_3(s)} \tag{8}$$

with

$$\Delta_r G = A_r + B_r T_{ref} = \overline{\Delta G}_{O_2}(T_{ref}) \tag{9}$$

and

$$2\mathrm{H_2O(g)} = 2\mathrm{H_2(g)} + \mathrm{O_2(g)}, \tag{10}$$

$$\overline{\Delta G}_{O_2}(T_{ref}) = 2RT_{ref}\ln(p\mathrm{H_2O}/p\mathrm{H_2})^\circ + A + BT_{ref}\log T_{ref} + CT_{ref}. \tag{11}$$

The partial Gibbs energy over the UO_2 sample at T (hot side of the ampoule) is calculated according to the same relation but with temperature T and the same ratio $(p\mathrm{H_2O}/p\mathrm{H_2})^\circ$:

$$\overline{\Delta G}_{O_2}(T) = 2RT\ln(p\mathrm{H_2O}/p\mathrm{H_2})^\circ + A + BT\log T + CT. \tag{12}$$

Replacing the $(p\mathrm{H_2O}/\mathrm{pH_2})^\circ$ ratio by its value in relation (12) and using relation (11) to eliminate $\overline{\Delta G}_{O_2}(T_{ref})$, we obtain,

$$\overline{\Delta G}_{O_2}(T) = A\left(1 - \frac{T}{T_{ref}}\right) + BT\log\frac{T}{T_{ref}} + \frac{T}{T_{ref}}\Delta_r G(T_{ref}). \tag{13}$$

Using this last relation and the published values of T_{ref} by Markin et al. [47], we effectively reproduced the results of the authors.

For the Wheeler and Jones [51] paper, T_{ref} – non-published – was calculated using relation (9) via a computer: $T_{ref} = 980$ K for $\overline{\Delta G}_{O2} = -152.0$ kcal, 989 K for −151.0 kcal and 1219.5 K for −130.2 kcal. These temperature values are necessary to build correction factors as well as to estimate the uncertainties. Correction factors are presented in Table 4 on the basis of these relations and by reference to JANAF 1998 tables.

3.2.2. Temperature uncertainty estimates

For pyrometric measurements [45–51], the stability of the temperature control added to the pyrometric readings and necessary calibration procedures lead to $\delta T \sim \pm 15$ K. For W/Re thermocouples [52], we would prefer to increase slightly the estimates of the authors up to $\delta T = \pm 10$ K.

3.2.3. Composition uncertainty estimates

For composition analysis by air oxidation and also calcinations [45,46,48,52] into U_3O_8, we apply the Ackermann and Chang [68] correction as already explained by Labroche et al. [3] because the calcination temperature is higher than 873 K. When not specified [45,46,48] we have arbitrarily chosen to be in the range 1173–1223 K, the usual range employed at the time of the studies. Half of the correction value is used to correct the authors original composition results, the second half part is included in the uncertainty estimates. The following relation is used to evaluate the total composition uncertainty:

$$\delta(\mathrm{O/U}) = [(\text{half correction})^2 + (\text{air exposure})^2 + (\text{graph readings})^2 + (\text{authors reproducibility})^2]^{1/2}. \tag{14}$$

The authors reproducibility is generally considered as the authors uncertainty as published. A summary of our estimated (O/U) uncertainties is presented in Table 5.

For studies performed with $CO/CO_2 = 10/1$ gaseous flow equilibrium compositions, Markin et al. [47], Wheeler [50] and Wheeler and Jones [51], the final composition is located in the oxygen potential vertical change in stoichiometric UO_2. This composition was estimated first by the authors [47,50] to be very accurate, $\approx \pm 0.001$ and later to be ± 0.003 (see Fig. 2 in [51]), but as the comparison with other methods, like H_2/H_2O flow ratios or hydrogenation into UH_3, gives results to within 0.005 [51], we adopt a total uncertainty $\delta(\mathrm{O/U}) = \pm 0.005$. As the silica sheath is opened in an argon filled glove box, and the sample is firstly slightly oxidized to UO_{2+x} by a known amount of O_2 (volumetric

Table 5
Composition uncertainty estimated in this work δ(O/U), for heterogeneous equilibrium methods

Authors [Refs.]	Calcination correction[a] for O/U authors ratio	Uncertainty causes				δ(O/U), our estimates
		Calcination	Air exposure	Graph readings	Authors estimates	
Aitkin et al. [45]	−0.0142	0.0142	0.002	–	0.003	±0.0145
Alexander et al. [46]	−0.0142	0.0142	0.002	–	0.01	±0.0175
Tetenbaum and Hunt [48]	−0.0142	0.0142	0.002	0.25	–	±0.0145
Javed [52]	−0.0107	0.0107	0.002	–	0.003	±0.0113
Markin et al. [47]	–	–	–	–	0.005	±0.005
Wheeler [50] Wheeler and Jones [51]	–	–	–	–	0.005	±0.005

[a] Due to incomplete recovering of the U_3O_8 composition according to Ackermann and Chang data [68] as explained in text.

method) before reduction, there is no uncertainty due to air exposure (see Table 5).

3.2.4. Oxygen Gibbs partial energy uncertainties

The total uncertainty is calculated when adding the uncertainty associated with the reference equilibrium to that for the measured values which are usually of pressure ratios. Each of these uncertainties has to be calculated according to the sequence of relations used in the calculation of $\overline{\Delta G}_{O_2}$.

For the reference equilibrium, we use the uncertainties quoted in JANAF 1998 tables for enthalpies of formation and entropies of the components as for instance:

$$2H_2 + O_2 = 2H_2O \tag{15}$$

$$\delta(\Delta G_{ref}) = \delta\Delta_f H^{O}_{H_2O} + T(\delta S^{O}_{O_2} + 2\delta S^{O}_{H_2} + 2\delta S^{O}_{H_2O}) \tag{16}$$

The uncertainties as calculated for each reference or intermediate equilibrium are quoted in Table 6. The uncertainty associated with the measured quantities are quoted also in Table 6 and are estimated either according to authors estimates [45,46] or by analogy with earlier and similar works: for example, an uncertainty of 5% for p_{H_2O} [48] and an arbitrary 1% for carrier gas H_2, or flow meters for p_{CO} and p_{CO_2}. In Markin et al. [47] and Wheeler and Jones [51] equilibration method with Cr/Cr_2O_3 or Nb/NbO, the uncertainty is only depending on the cold reference temperature T_{ref}: authors proposed ± 2 K, but we generally prefer ± 5 K for thermocouples below 1300 K (intrinsic uncertainty of the thermocouple, of the reference temperature and those associated to the positioning close to the sample). The uncertainty for the Gibbs energy is calculated by combining in relation (12) the uncertainty from references data and from T_{ref}, using a summation analogous to the law of propagation of errors since the number of uncertainty causes is large and may probably statistically tend to cancel:

$$\delta\left(\overline{\Delta G}_{O_2}\right) = \left[\delta\left(\overline{\Delta G}_{O_2}\right)^2_{ref} + \delta\left(\overline{\Delta G}_{O_2}\right)^2_{meas}\right]^{1/2} \tag{17}$$

with

$$\delta\left(\overline{\Delta G}_{O_2}\right)^2_{ref} = [\delta\Delta G^{T}(H_2O/H_2)]^2 + \left[\frac{T}{T_{ref}}\delta\Delta G^{T_{ref}}(Cr/Cr_2O_3)\right]^2 + \left[\frac{T}{T_{ref}}\delta\Delta G^{T_{ref}}(H_2O/H_2)\right]^2 \tag{18}$$

and

$$\delta\left(\overline{\Delta G}_{O_2}\right)^2_{meas} = \left[(5516 + 0.995T_{ref})\frac{T}{T^2_{ref}}\delta T_{ref}\right]^2 \quad \text{for } Cr/Cr_2O_3 \tag{19}$$

or

$$\delta\left(\overline{\Delta G}_{O_2}\right)^2_{meas} = \left[(25\,116 + 17.415T_{ref})\frac{T}{T^2_{ref}}\delta T_{ref}\right]^2 \quad \text{for Nb/NbO.} \tag{20}$$

The impact of thermal diffusion as estimated by Markin et al. [47] may decrease the H_2O pressure by a factor 4 and consequently the partial Gibbs energy of O_2 increases by a factor $0.25RT$(3000–5000 J). This factor 4 was not measured when checking with Ar/H_2 mixtures because the impact on the final O/U ratio as analysed at $O/U = 2 \pm 0.005$ is not sensitive enough when converted into $\delta\overline{G}_{O_2}$.

The total uncertainty of the isopiestic method as used by Markin et al. [47] can be checked by comparison of those measurements performed at 1600 and 1700 K for $O/U > 2.02$, as shown in Fig. 10, with the array values as retained in the previous study of Labroche et al. [3]. We observe a systematic trend that can be as large as 10 000 J. This shift will

Table 6
Oxygen partial Gibbs energy uncertainties as estimated in this work for heterogeneous equilibrium methods

Authors [Refs.]	Reference equilibrium and uncertainty	Measurement uncertainties	Total uncertainty $\delta(\overline{\Delta G}_{O_2})$ (J)
Aitken et al. [45]	$2H_2 + O_2 = 2H_2O$ $\delta(\Delta G_{ref}) = 84 + 0.187T$	$\delta p_{H_2O}/p_{H_2O} \sim 0.5$ $\delta p_{H_2}/p_{H_2} = 1\%$ $\delta(\Delta G_{meas}) = 8.48T$	$84 + 8.67T$
Alexander et al. [46] Javed [52]	ditto	$\delta p_{H_2O}/p_{H_2O} = 5\%$ $\delta p_{H_2}/p_{H_2} = 1\%$ $\delta(\Delta G_{meas}) = 0.9977T$	$84 + 1.185T$
Tetenbaum and Hunt [48]	$O + H_2 = H_2O$ and $O_2 = 2O$ $\delta(\Delta G_{ref}) = 384 + 0.0272T$	$\delta p_O/p_O$(graph) $= 0.15$ $\delta p_{H_2O}/p_{H_2O} + \delta p_{H_2}/p_{H_2} = 0.06$ $\delta(\Delta G_{meas}) = 3.49T$	$384 + 3.76T$
Markin et al. [47]	$4/3\ Cr + O_2 = Cr_2O_3$ $\delta(\Delta G_{ref}) = 5600 + 1.18T_{ref}$	$\delta T_{ref} = \pm 5$ K	$(5516 + 0.995T_{ref})\frac{T\delta T_{ref}}{T^2_{ref}}$
	$2Nb + O_2 = 2NbO$ $\delta(\Delta G_{ref}) = 25200 + 17.6T_{ref}$	$\delta T_{ref} = \pm 5$ K	$(25116 + 17.415T_{ref})\frac{T\delta T_{ref}}{T^2_{ref}}$
	$2H_2 + O_2 = 2H_2O$ $\delta(\Delta G_{ref}) = 84 + 0.185T$ (or T_{ref})	$\delta T_{ref} = \pm 2$ K applied in relation (11)	Combination of uncertainties in the propagation law of error (see text; relations (17)–(20)). The total uncertainty is obtained when adding: • Thermal diffusion $\overline{\delta G}_{O_2} = 5000$ J • Comparison with other measurements (our array in Ref. [3]) at O/U > 2 (see text): $\overline{\delta G}_{O_2} = 10000$ J
Wheeler [50]	$2C + O_2 = 2CO$ $\delta(\Delta G_{ref}) = 170 + 0.535T$	$\delta p_{CO}/p_{CO} = 5\%$ $\delta(\Delta G_{meas}) = 0.831T$	$170 + 1.366T$
Wheeler and Jones [51]	• H_2/H_2O same as Aitken et al. [45]	$\delta p_{CO_2}/p_{CO_2} = \delta p_{CO}/p_{CO} = 1\%$	$440 + 0.687T$
	• $2CO + O_2 = CO_2$	$\delta(\Delta G_{meas}) = 0.332T$	
	• $\delta(\Delta G_{ref}) = 440 + 0.355T$	Same as Wheeler [50]	$170 + 1.366T$
	• C/CO/UO_2 same as Wheeler [50]	Same as Ref. [47] $\delta T_{ref} = \pm 5$ K	$(5516 + 0.995T_{ref})\frac{T\delta T_{ref}}{T^2_{ref}}$
	• H_2/H_2O sealed Cr/Cr_2O_3 Same as Markin et al. [47]		

be retained as an additional uncertainty (see Figs. 21 and 22).

Among transport studies, Alexander et al. [46] used also the chemical analysis of U bearing species after condensation from the Ar carrier gas at the exit of the equilibration chamber, especially for a high oxygen content sample, namely $UO_{2.03}$. The oxygen potential was deduced from the UO_3/UO_2 gaseous equilibrium, but the data for UO_3(g) are so controversy (see for instance our report [70] including new data obtained after the Alexander et al. work) that we prefer to let these data aside. Indeed, a direct comparison of the Alexander et al. data (Fig. 11) for O/U = 2.0158 with the interpolated array values from Labroche et al. [3] shows large discrepancies.

3.3. Knudsen cell and mass spectrometric determinations

Combination of Knudsen cell and mass spectrometric methods, either run in two independent and complementary experiments [58] or coupled in the same apparatus [59–64] have been used with the main advantage of being able to analyse the gas phase composition. This gas phase consists of the following species, U(g), UO(g), UO_2(g) and UO_3(g). The main differences between authors depends on the modes of calibration of the mass spectrometers in order to relate ionic intensities of observed ions to partial pressures using the basic mass spectrometric relation,

$$p_i S_i = \mathrm{I}_i^+ T \tag{21}$$

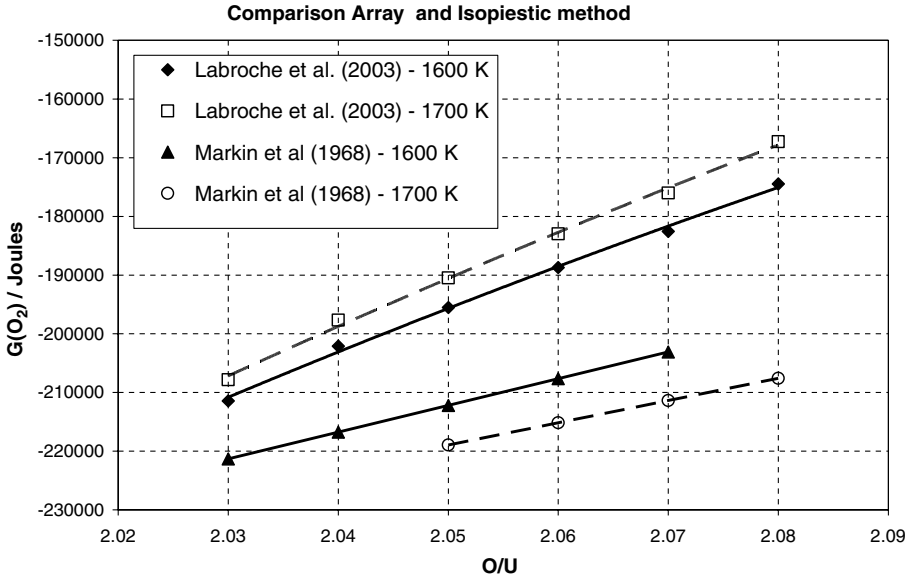

Fig. 10. Comparison of Markin et al. [47] determinations of the oxygen Gibbs energy performed by the isopiestic method (Cr_2O_3) (Cr Ref. system) with array values as retained in the preceding work of Labroche et al. [3].

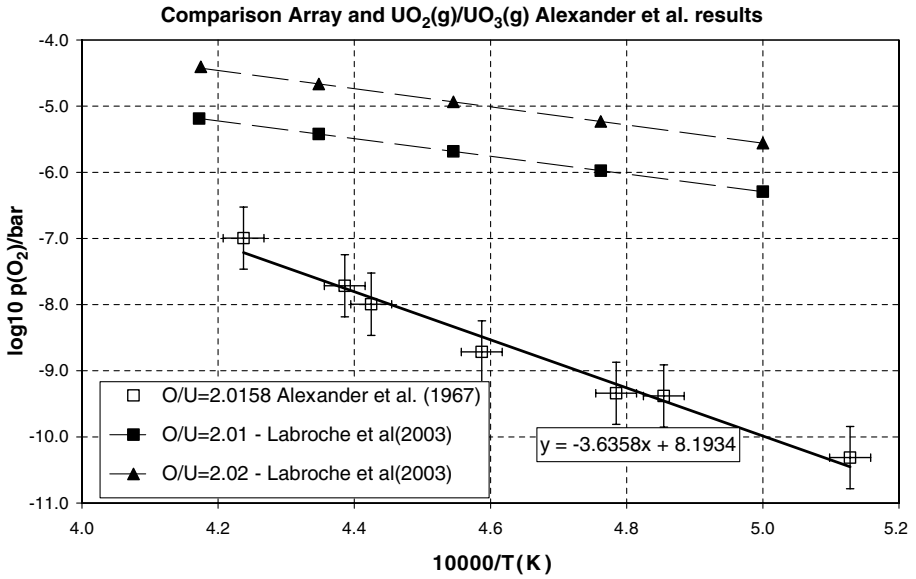

Fig. 11. Comparison of Alexander et al. [46] determinations of the Gibbs energy of oxygen performed by the H_2O/H_2 flow method and deduced from the UO_3/UO_2 equilibrium with array values as retained in the preceding work of Labroche et al. [3].

in which p_i is the partial pressure of the i species in the Knudsen cell, S_i the mass spectrometric sensitivity for this species, I_i^+ its measured ionic intensity, and T the cell temperature.

This relation is usually written in a simplified form for the sensitivity:

$$S_i = A\sigma_i(\mathrm{eV})\gamma_i f_i \tag{22}$$

in which A is a geometrical factor, in principle, the solid angle subtended by the effusion orifice and the ion source aperture, – considered as a constant during an experiment, σ_i the ionization cross-section at the energy of the incident electrons (eV), γ_i the detector yield and f_i the isotopic abundance. All these factors are not always well-known [71] and rules for estimates have been either established or

assumed. A recent publication summarized these practices and evaluate the associated uncertainties [72]. Indeed, these uncertainties may have a non-negligible impact when thermodynamic data are determined for condensed phases, which we try to analyse in this paper.

In order to avoid interferences between parent ions (for example, U^+ from U(g)) and fragment ions (for example U^+ from UO(g)), measurements were performed for ionisation energies lower than the threshold for appearance of fragment ions, that is some 3–4 V above the ionisation potential of each species. An extrapolation to real ionic intensities at the maximum of the ionisation efficiency curve, which is generally at about 3–5 times the ionisation potential, has to be made since the ionisation cross-section estimates are more reliable for this maximum value. Errors may be generated in this extrapolation that have been later measured in the thesis work of Younés [73]. The whole set of ionisation patterns of the different uranium gaseous oxides has been determined and the relative ionisation cross-section at their maximum measured for UO_3/UO_2; this study is extensively summarized in a CEA report [70]. These results explain partly the disagreement of some of the original mass spectrometric results of Ackermann et al. [58] and of Pattoret, Drowart, Smoes [59–62] relating to the gaseous phase thermodynamic data. For this reason, our analysis of oxygen activities as well as uranium activities in this paper will be conducted in a self-consistent manner, that is by using for each authors their own references (calibrations, secondary data if necessary...) because the introduction of external data may enlarge the present scatter between different authors.

A second source of uncertainties or systematic errors comes from the chemistry of uranium, its complex gas phase and its reactivity with containment materials. As shown early by Pattoret and coworkers, Ta Knudsen cells seem less suitable than W cells in the hypostoichiometric UO_{2-x} range because oxygen can more easily be dissolved in Ta and diffuse through the cell walls, and uranium can also creep out of cells or cause intergranular penetration of cell walls [59,61]. This behaviour may affect the calibration procedure when based on total mass loss or on target collection since as shown by Pattoret the gas phase in the presence of Ta cells appears less rich in gaseous oxides of higher oxidation states. The reactivity of the U–O system is also relevant outside the effusion cells, since many authors observed parasitic molecular flows additional to the genuine effusion flow that is the only flow appropriate to the studied equilibrium. In original and earlier mass spectrometric devices, as for instance in the study of gaseous U–O system, De Maria et al. [74] observed with a mobile slit interposed between the effusion orifice and the ion source aperture that surface vaporizations (Fig. 12(c)) contributed to the detected flow; the more reducing the original vapour, the more additional contribution was observed. Pattoret, Drowart and Smoes [59–62] (Fig. 12(a) and (b)) observed the same behaviour and further used these analysis of the molecular beam distribution systematically in order to select their best conditions for measurements: data showing some anomalous surface vaporizations were systematically discarded. Storms [63] observed also some 'thermal shields' surface contributions for

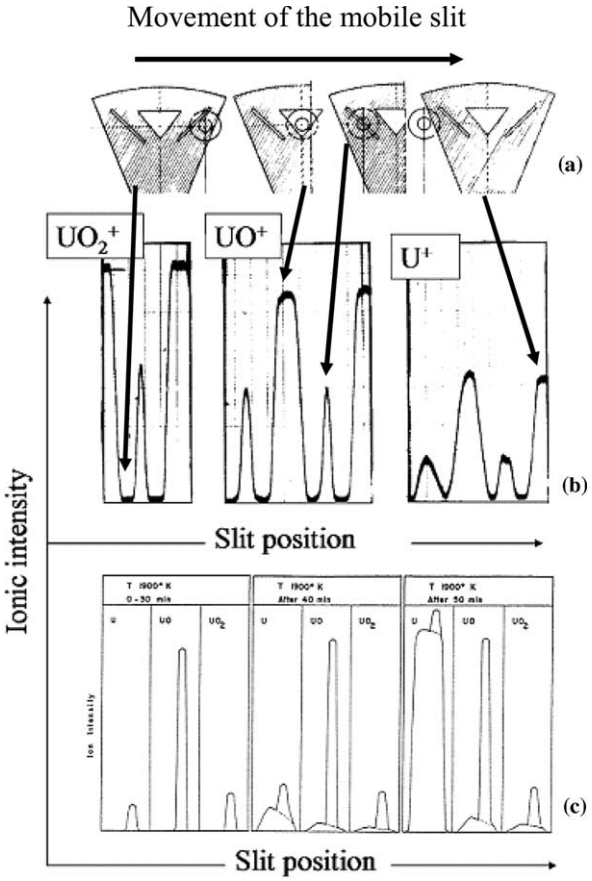

Fig. 12. Parasitic surface evaporations as observed in the study of the U–UO_2 system by Knudsen-cell mass spectrometry using a mobile slit profile device: (a) from de Maria et al. [74]; (b) from Pattoret and coworkers [59–62].

U(g), and some UO_2 'photo effect contributions' due to deposits at high temperature in conjunction with electron bombardment heating of the furnace device.

These surface contributions to the measured molecular beam – the part of the molecular beam that is ionized in the ionization chamber of the mass spectrometer – have been analysed by Chatillon et al. [75] and the main conclusions are:

- A quite constant proportion of surface vaporization relatively to the actual effused beam is coming from the steady state condensation/evaporation on thermal shields and from the external cell surface around the effusion orifice. These proportions can be changed by oxidation or deoxidation with surface reactions depending on the cell and furnace materials together with the quality of the vacuum system. Usually as observed by De Maria et al. [74], Pattoret, Drowart and Smoes [59,61,62], and Storms [63] these contribution for the U–O system are more pronounced for reductive species ($U > UO > UO_2$). Indeed Pattoret and coworkers did not detect any contribution for $UO_2(g)$, with their mobile slit device, and the UO_2 'slit profile' served as a reference (see Fig. 12(b)) for negligible surface vaporization.
- A localized contribution from the effusion orifice edge due to surface diffusion from species adsorbed on the inner walls of the effusion cell. These inner adsorbed species correspond to an equilibrium state with the sample, meanwhile outside the chemical potential becomes very low due to vacuum pumping and elimination of effused molecules by condensation on the cold parts of the furnace. Thus a large chemical potential gradient exists between the inner and outer faces of the effusion orifice that favours the surface diffusion flow along the orifice walls. Simulation as carried out by Chatillon et al. [75] showed that these contributions, which can amount to 10–20%, are not easy to detect with the mobile slit device because they are localized at the orifice edge. Winterbottom et al. [76] showed that this phenomenon in competition with effusion, due to differences in activation energies, becomes less important as temperature increases: this feature leads to a decrease of vaporization enthalpies as obtained from second law calculations.
- A third phenomenon as observed frequently with U(l) is the creeping of the liquid along the effusion orifice walls, especially when deoxidation becomes efficient by preferential vaporization of UO(g). In a first step the surface diffusion increases, but very suddenly above some temperature threshold, creeping is occurring. The mobile slit device is very efficient for determining this onset as shown by De Maria et al. [74] and Pattoret et al. [59–62]. The effect of the creeping on second law results is the reverse of the surface diffusion effect. Thus in the U–O case when U(l) is analysed, we cannot decide upon the origin of the trend in the slopes as observed by Storms [63]. What we can ascertain is that these parasitic contributions, as analysed in the technical IUPAC report [72] on mass spectrometry, lead to larger uncertainties in second law calculations than in third law calculations.

Later, in the course of methodological studies of the twin and multiple cell techniques [77–79], Morland et al. [80] proposed a restrictive collimation device that definitely eliminated any detection of surface flows since the molecular beam sampling by the ion source is achieved by 'viewing' inside the effusion orifice. It is this solution that has been used recently by Baïchi et al. [64] for the study of UO_2 activity in the U–UO_{2-x} diphasic domain.

In the following data analysis and for estimating their uncertainties, these above mentioned features will be discussed in the data selection as well as for uncertainties evaluation.

3.3.1. Diphasic UO_{2-x}–U(l) domain

In earlier times, at the beginning of the U–O system investigations, a long debate was centered upon the oxygen solubility in liquid uranium that would have influenced the vapor pressure measurement of the diphasic UO_{2-x}–U(l). Activity measurements for uranium by Pattoret and coworkers [59–61] showed a small tendancy to decrease for $T \geqslant 2100$ K. Uncertainty limits overlap the uranium activity decrease from pure uranium – and our recent analysis of solubility data [2] led to retain very small values, two features that are in favour of classical Raoult law for liquid uranium. For oxygen activity, the first determinations [58–62] were based on the equilibrium,

$$UO_2(g) \leftrightarrows \Delta UO(g) + O(g) \tag{23}$$

from which the O pressure (not measured) was deduced by direct measurements of partial pressures of UO(g) and UO_2(g) over the diphasic UO_{2-x}–U(l) (supposedly UO_2–U (l, pure)).

In terms of total absolute uncertainties, the formation enthalpies of UO_2(g) and UO(g) are, according to the authors, ± 15 kJ, and their entropies for UO(g) ± 6.5 J K^{-1} mol^{-1} and for UO_2(g) ± 10.5 J K^{-1} mol^{-1}. Neglecting those uncertainties associated with O(g) thermodynamic data (see Janaf tables) the uncertainty of the Gibbs energy of reaction (23) can be calculated as:

$$\delta(\Delta_r G) = \sqrt{\delta\Delta_f G(\mathrm{UO},g)^2 + \delta\Delta_f G(\mathrm{UO_2},g)^2} \quad (24)$$

or

$$\delta(\Delta_r G) = \sqrt{\delta\Delta_f \mathrm{H}(\mathrm{UO},g)^2 + \delta\Delta_f \mathrm{H}(\mathrm{UO_2},g)^2} + T\sqrt{\delta S^{\circ}(\mathrm{UO},g)^2 + \delta S^{\circ}(\mathrm{UO_2},g)^2} \quad (25)$$

when assumptions are made that some compensation effects may occur. Thus the uncertainty associated with the Gibbs energy of O(g) becomes:

$$\delta\left(\overline{\Delta G}(\mathrm{O})\right) = 21\,200 + 12.02T \quad (26)$$

that gives, neglecting the uncertainty in the O_2 dissociation:

$$\delta\left(\overline{\Delta G}(\mathrm{O_2})\right) \cong 42\,400 + 24.4T. \quad (27)$$

We quote that this uncertainty, as usually admitted for determinations of formation enthalpies of gases, leads to large uncertainties in the determinations of condensed phases thermodynamic properties. For these reasons, mass spectrometrists developed [77,82] different methods to obtain more accurate activity determinations. For the study of the diphasic U(l)–UO_{2-x}, Pattoret and coworkers [59–62] used a twin Knudsen cell method, meanwhile Baïchi et al. [64] a multiple cell method: respectively two and four Knudsen-cells (crucible + lid) are located in a unique and isothermal envelope, and a mobile furnace allows successive measurements to be performed in a short time sequence for the same ionic intensity (or partial pressure) coming from different samples located in the different cells or compartments.

The determinations were made via the partial pressure decrease of UO_2(g) in equilibrium with the diphasic UO_{2-x}–U(l) relatively to pure UO_2 as reference, stoichiometric or slightly hyperstoichiometric at the congruent composition that is relatively stable to vaporization.

Initially, the partial pressure difference between UO_2 stoichiometric and congruent was measured to be 0.965 ± 0.035 [59,60], which is quite small considering the uncertainty limits. With the twin or multiple cell methods the sensitivity of the mass spectrometer cancels and consequently does not need to be evaluated and thus eliminates a cause of uncertainty. The main studied reaction is:

$$\mathrm{UO_2(solid,\ solution)} = \mathrm{U(l)} + \mathrm{O_2(g)} \quad (28)$$

for which the equilibrium constant is,

$$Kp = \frac{a(\mathrm{U};l)\cdot p_{\mathrm{O_2}}(\mathrm{g})}{a(\mathrm{UO_2},sol.sol)} \quad (29)$$

and with the accurately known Gibbs energy of formation of UO_2(s):

$$RT\ln \mathrm{K}p = -\Delta_f G^{\circ}_{\mathrm{T}}(\mathrm{UO_2},s) \quad (30)$$

and

$$\overline{\Delta G}_{\mathrm{O_2}} = \Delta_f G^{\circ}_{\mathrm{T}}(\mathrm{UO_2},s) + RT\ln\frac{a(\mathrm{UO_2})}{a(\mathrm{U})} \quad (31)$$

relation in which a (UO_2) is the measured ionic intensity ratio of UO_2(g), and $a(\mathrm{U}) \cong x(\mathrm{U})$ (Raoult's law). Accurate measurements of ionic intensity ratios of UO_2(g) lead to a small uncertainty, ≈2800–3000 J mol^{-1}, as explained by Baïchi et al. [64]. This uncertainty is at least 10 times lower than the usual ones given for gas phase determinations. Baïchi et al. [64] completely confirmed the earlier measurements by Pattoret and Coworkers [59–62] and had to reject the data of Ackermann et al. [58,81].

In conclusion, we retain the Pattoret, Drowart and Smoes [59–62] data with their proposed uncertainties and the Baïchi et al. [64] values as mentioned in their Table 2. We have to state that these values are pertinent only in the $2000 < T < 2300$ K range, since for lower temperatures the UO_2 activity is equal to one. Taking into account of the small uncertainty associated with the Gibbs energy of formation of UO_2(s), we observe that the partial Gibbs energy of oxygen is now well-known for the diphasic U–UO_2 domain, which somehow constrains phase relations for the liquidus shape.

For temperature uncertainties, we retain those quoted by the authors: ±15 K [59–62] for pyrometry and ±10 K [64] for W/Re thermocouples.

3.3.2. Monophasic UO_{2-x} hypostoichiometric domain

Partial Gibbs energies of uranium and of oxygen were measured by mass spectrometry [59–63] either directly by determinations of U(g) partial pressures

or indirectly via equilibrium constants between UO_x gaseous species. Indeed, as published by Pattoret and coworkers [59,61], the evolution of the different partial pressures at constant temperature as a function of O/U ratio are very significant, but there exists always several species in the gas phase that are detectable together and this feature allows the determination of uranium or oxygen activities in the complete composition range.

3.3.2.1. Composition uncertainties. Pattoret and coworkers [59–61] performed experiments with mass loss calibration (in addition of silver reference calibration) and analysed their samples before and after experiments by polarography. They propose an uncertainty of ±0.0003 for this technique and a total uncertainty for their compositions of ±0.005. Some samples were analysed also for their oxygen surface composition, richer in oxygen by +0.003 than for bulk composition. Moreover, the authors estimated the oxygen diffusivity of their W cells to lead to an uncertainty on their O/U ratio of ±0.003 [60], the value to be applied to their mass loss uncertainty. Applying our criteria (Table 1 in Ref. [2]) for the polarographic technique, and the propagation law of errors we calculate,

$$\delta(\mathrm{O/U}) = \sqrt{(0.005)^2 + (0.005)^2 + (0.003)^2} = \pm 0.0077 \quad (32)$$

value slightly larger than proposed by the authors. We retain our value estimated above.

Storms [63] analysed his samples by combustion in O_2 at 950 °C and with the assumption of stoichiometric U_3O_8 formation. As discussed in a preceding paper [3], and according to Ackermann and Chang [68], for this relatively high temperature, the U_3O_8 compound is not stoichiometric. We propose to shift the Storms 'as published' compositions by $\delta x = -0.0132$ (half the 'Ackermann and Chang' correction) and to keep the second half part as the uncertainty.

A criteria for the validity of these corrections as well as of the evaluation of the total uncertainties, may be established as proposed by Storms when comparing directly the partial enthalpies of vaporization for the UO(g) – this species being often the predominant one in the composition range analysed by mass spectrometry – as presented in Fig. 13 that

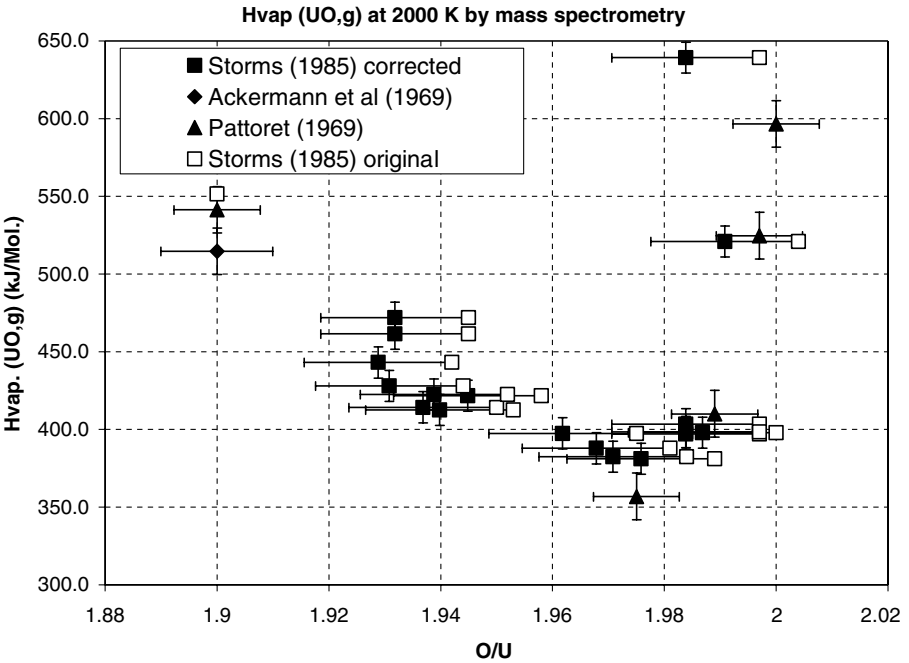

Fig. 13. Partial vaporization enthalpies as measured – second law method – for the UO(g) species in Knudsen cell mass spectrometry as a function of composition in the UO_{2-x} hypostoichiometric domain, and for the diphasic U(l)–UO_{2-x} (O/U = 1.9). Ackermann et al. [58], Pattoret and coworkers [59–62] and Storms [63]. Storms 'corrected' corresponds to a correction for the analysis of the O/U composition due to the incomplete calcinations into U_3O_8 (see text).

includes uncertainty bars. This figure is the same as Fig. 5 in Storms [63]. We observe that the correction applied to Storms composition values leads to better agreement with Pattoret and coworkers partial vaporization enthalpy values, especially for the minimum value of this partial vaporization enthalpy (slopes from second law results). Values for O/U ~ 2 are less accurate since the influence of composition uncertainties is much larger than the real uncertainty applied to the slopes. In this figure we apply a ± 15 kJ mean value for the slopes uncertainty, this value being in agreement with the general uncertainty given by the authors when determining dissociation energy for UO(g) or formation enthalpy. During the following analysis of the uranium activity or partial Gibbs energy we also further observed that this correction led to an excellent agreement between the two studies (see Fig. 17 for example).

A second criteria is the comparison of the solidus phase limit obtained by the intersection (interpolated or extrapolated) of partial Gibbs energies measured for constant composition O/U and the partial Gibbs energy as measured by each author (for internal consistency reason) for the diphasic U–UO_{2-x}. These phase limits are compared with data retained in the preceding work [2] in Fig. 14. These limits were obtained by potentiometric analysis and are considered as secondary data. These data are consequently not always retained since it is difficult to ascertain their uncertainty ranges. Although Storms uses a specially constructed pyrometer [83] to determine the temperature with an accuracy of ± 2 K, the larger uncertainty observed for this phase limit as revealed by the scatter of the data must be attributed to the uncertainty in slopes (second law results). In fact, this uncertainty is related directly to difficulties in calibration procedures and to parasitic contributions that are not controlled. Comparing Pattoret and coworkers data with Storms original and corrected data, as shown in Fig. 14, leads us to confirm the validity of our proposed correction for the O/U ratios of Storms.

3.3.2.2. Partial Gibbs energies of uranium. The uncertainties associated with the vapor pressure of U(g) either directly measured or via other species depends on the kind of experiment and its management.

In their isothermal run at 2250 K, Pattoret and coworkers refer the U(g) partial pressure to a reference composition as measured at the beginning of the experiment. So, at 2250 K, the diphasic U(l)–UO_{2-x} is the reference for the uranium standard pressure and activities of uranium are then calculated all along the experiment when composition goes toward the congruent one close to UO_2 (see

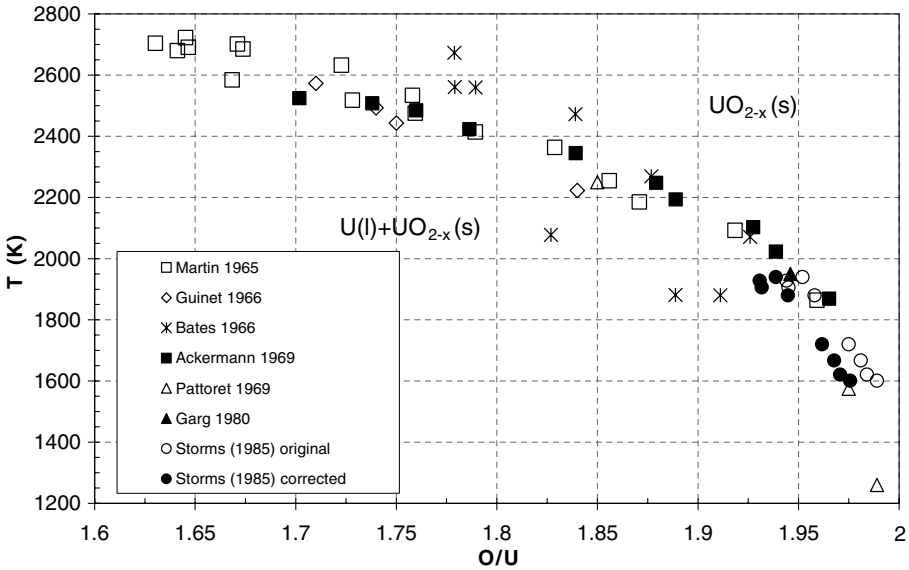

Fig. 14. Comparison of different solidus determinations for the UO_{2-x} hypostoichiometric domain. Potentiometric analysis were performed by Pattoret and coworkers [59–62] (oxygen Gibbs energy) and Storms [63] (uranium Gibbs energy). We observe a good agreement for Pattoret and coworkers with other kind of measurements (see our preceding work by Baïchi et al. [2]), meanwhile only Storms values with our correction for O/U composition agree.

Fig. 9.1, p. 156 in [59], or Fig. 6 in Ref. [61]). In this case, and for a stabilisation of the mass spectrometer which is considered as good enough in an experiment, we attribute a relative uncertainty of ±0.2 for intensity detection, and ± 0.2 for surface contributions, and finally,

$$\frac{\delta p_U}{p_U} = \sqrt{(0.2)^2 + (0.2)^2} = \pm 0.28 \quad (33)$$

and consequently

$$\delta \overline{G}_U = RT \times 0.28 = \pm 5200 \text{ J at } 2250 \text{ K}. \quad (34)$$

This uncertainty accounts only for $O/U < 1.95$ where U(g) was directly measured.

Other uranium activities – as published in the same figure, – come from gaseous equilibria, as for example,

$$UO_2(g) + U(g) = 2UO(g) \quad (35)$$

equilibrium for which the constant Kp is only temperature dependent. So, at 2250 K (isothermal run),

$$\frac{\delta p_U}{p_U} = 2\frac{\delta p_{UO}}{p_{UO}} + \frac{\delta p_{UO_2}}{p_{UO_2}} \quad (36)$$

and when evaluating the pressure uncertainties on the same basis,

$$\frac{\delta p_U}{p_U} = (2(0.2^2 + 0.2^2) + (0.2^2 + 0.2^2))^{1/2} = \pm 0.49 \quad (37)$$

and

$$\delta \overline{G}_U = \pm 0.49RT = \pm 9200 \text{ J}. \quad (38)$$

These two series of measurements isothermal and isochore runs are presented altogether in Fig. 15.

Pattoret and coworkers performed also experiments in which some sequences can be interpreted for constant composition. We extracted from tables in Ref. [59] different compositions (O/U ratios) as presented in Fig. 16, and some data for $O/U = 2$.

These five compositions are also presented and compared at 2250 K with those of the isothermal run in Fig. 15. As these activities are deduced from gaseous equilibria, we adopt the same uncertainty that proposed in relation (38). We observe in Fig. 15 that all these different determinations are in agreement. These data will be least square fitted to build our array.

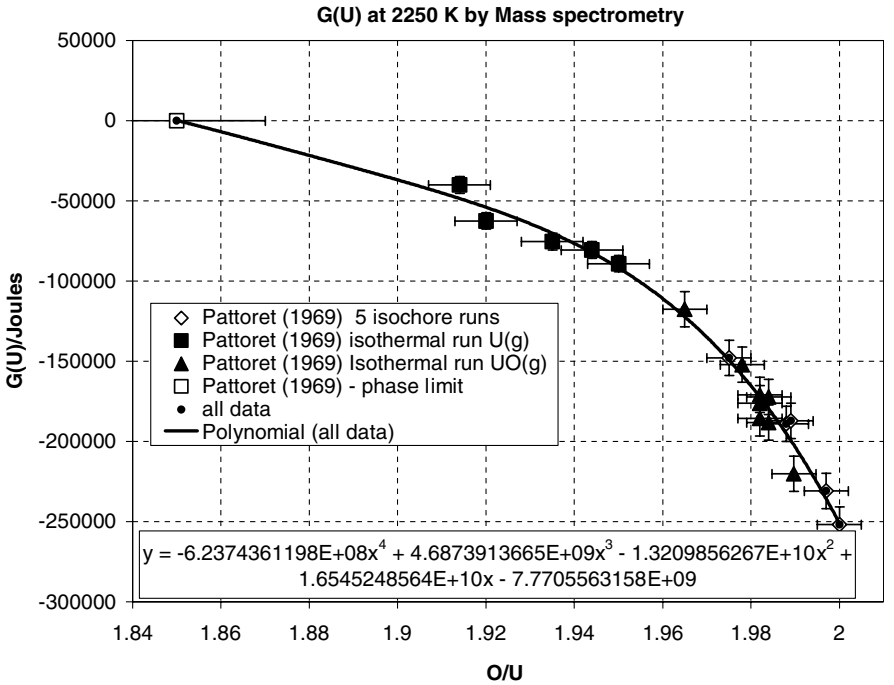

Fig. 15. Determinations of the partial Gibbs energy of uranium by Knudsen cell mass spectrometry [59–62] in two kinds of experiments, – isothermal and isochore runs. These experiments performed independently, and each of them with their associated calibration method, agree within our estimated uncertainty range.

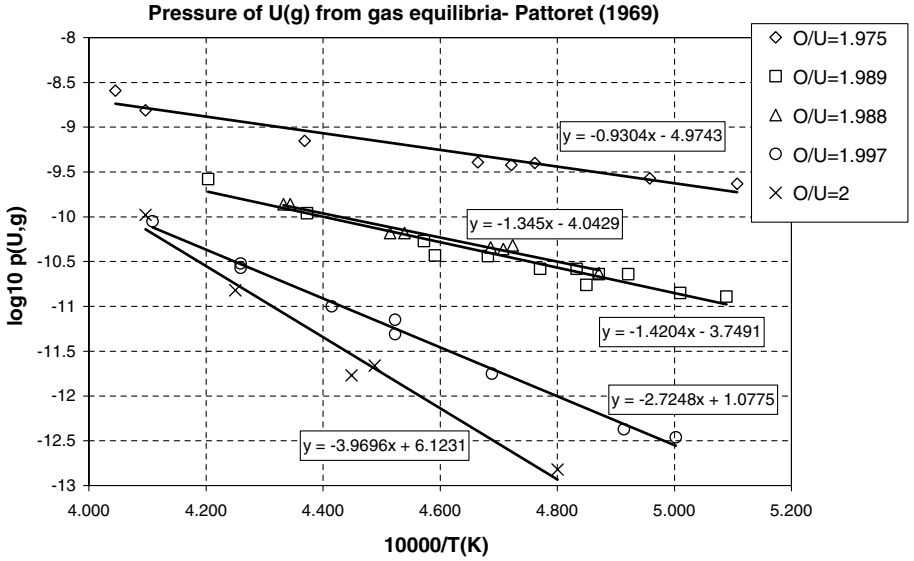

Fig. 16. Least square fits of vapour pressure of U(g) as determined by Pattoret and coworkers [59–62] in equilibrium with UO_{2-x} at five different O/U ratios. These data were obtained in mass spectrometry using equilibrium constants between the different gaseous species UO(g), UO_2(g) and UO_3(g) as determined in these different experiments.

Storms [63] determined activity of uranium either by direct measurements of U(g) pressure or using equilibrium relation (35) with the double assumption that, for comparison of two experiments at the same temperature, Kp is constant, and the pressure of UO_2(g) is a constant whatever is the composition in the UO_{2-x} domain. This last assumption remains valid for $T < 2100$ K as shown in the preceding part dealing with the U–UO_{2-x} diphasic domain and quite exact for Storms experiments that have been run in the 1667–2175 K range. The uncertainty in these measurements is associated to the determination of only one partial pressure – U(g) or UO(g) and we apply relation (33) but for the reference U–UO_2 and for the measured composition since these two values are obtained in different experiments:

$$\delta\overline{G}_{\mathrm{U}} = 2 \times 0.28RT \cong 10\,000 \text{ J}. \tag{39}$$

Thus we treated the two mass spectrometric studies in the same manner and assuming that there is no major source of another kind of errors like systematic errors. Indeed, for different temperature cross-sections – 1950, 2000, 2100, 2200 – the comparison of these two studies shows a good agreement as illustrated in Fig. 17, except for some Storms values close to O/U = 2 (1.985 and 1.991 as corrected). We observe also that, owing to the rapid variation of the Gibbs energy, the main source of disagreement resides on the O/U composition knowledge and its uncertainty, especially for O/U ratios close to UO_2 for which the Gibbs energy falls abruptly. For all these measurements, the correction applied to the Storms's compositions lead to an excellent agreement with Pattoret and coworkers data, which was not the case when comparing directly original values.

3.3.2.3. Partial Gibbs energy of oxygen. The partial Gibbs energy of oxygen, $\overline{G}_{\mathrm{O}_2}$, either obtained from isothermal or isochore mass spectrometric runs, are presented together at 2250 K in Fig. 18. As the gaseous species are the same as for $\overline{G}_U$ calculations, the associated uncertainties are the same. We observe in Fig. 18 that the two kinds of experiments are consistent within the uncertainty limits and are all retained to build the array values from these results. The four isochores experiments correspond to O/U = 1.975, 1.989 1.997 and 2.000 (Table 5 in Ref. [59]).

Questions can be raised about the simultaneous calculations of $\overline{G}_{\mathrm{U}}$ and $\overline{G}_{\mathrm{O}_2}$ from the same set of gaseous species U(g), UO(g), UO_2(g) and UO_3(g) and the necessary independence of these two partial Gibbs energy determinations. In fact the simultaneous measurements of at least two or more gaseous species allow the determination of at least two chemical potentials and for this reason we retain the two data sets, $\overline{G}_{\mathrm{U}}$ and $\overline{G}_{\mathrm{O}_2}$.

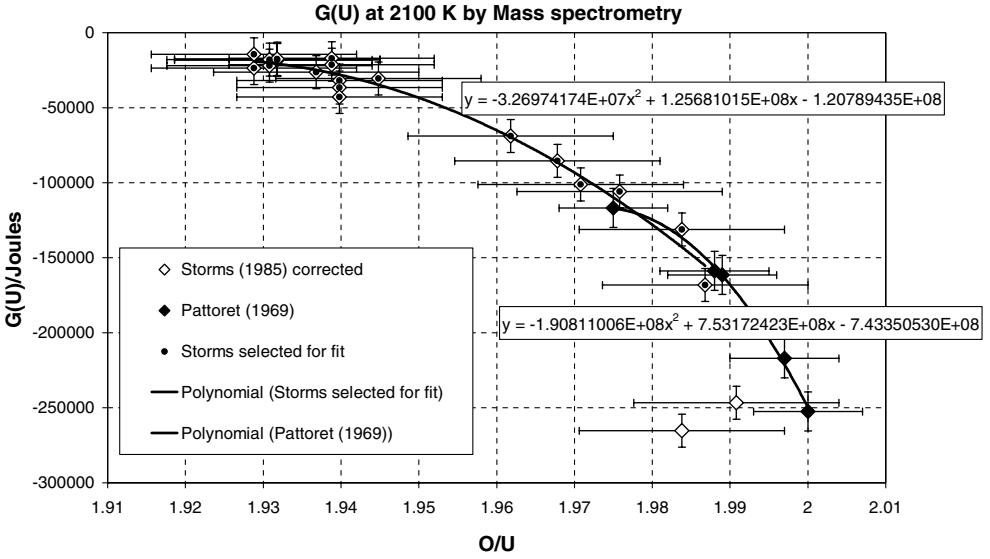

Fig. 17. Partial Gibbs energy of uranium as measured by Pattoret and coworkers [59–62] and Storms [63] by mass spectrometry at 2100 K. Storms corrected corresponds to original data, the O/U ratio being shifted by − 0.0133 as explained in the text for incomplete calcinations into U_3O_8.

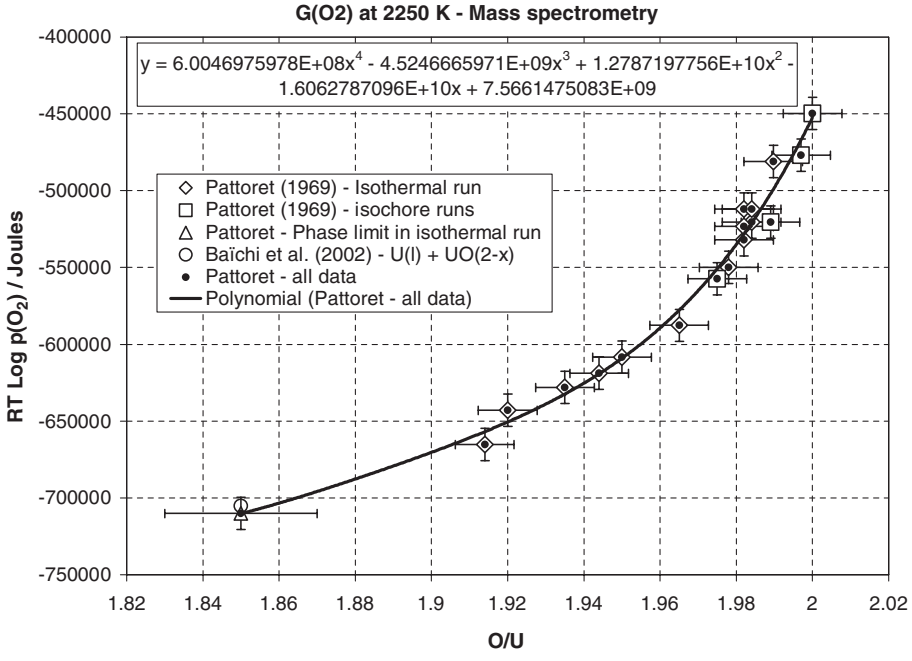

Fig. 18. Partial Gibbs energy of oxygen as measured by mass spectrometry: Pattoret and coworkers [59–62] in isothermal and isochore experiments, Baïchi et al. [64] with the multiple cell method.

4. Array data and intercomparison of different works

In some cases, published data can be compared directly, but generally this is not possible since the three raw data set ($\overline{G}_{O_2}$, O/U, T) do not necessarily overlap in the different studies. For this reason, as it was done by Labroche et al. [3] for the UO_2–U_3O_8 domain, we built an array of these values as

redistributed along regular steps. Two criteria are important in this distribution:

- the new data of the array remain included within the experimental limits since we do only an interpolation based on least square fits; moreover in any case we increase the number of data,
- the uncertainties as evaluated earlier are attributed to this new data set and we do not use the statistical parameters of any least square fit in order to decrease the original uncertainty.

According to the way used by the authors – isothermal runs or isochore runs – we fit the $\overline{G}_{O_2}$ published values in order to re-distribute the data along array values as shown for Tetenbaum and Hunt [48] in Fig. 19 for $T = 2705$ K. The repartition of the array data takes into account of the original density of data.

For compositions close to O/U = 2 where the uncertainties impact due to composition is much greater than those associated with $\overline{G}_{O_2}$ or $\log p_{O_2}$ due to the steep gradient of the Gibbs energy, comparison of different authors may be made at constant composition as a function of temperature. Disagreement in data between authors will reveal, first of all, composition disagreements or unidentified causes of composition uncertainties. As an example, Fig. 20 shows a very good agreement between e.m.f. determinations of Markin and Bones [53] and heterogeneous equilibria data of Wheeler and Jones [51] data different from the slopes deduced from Baranov and Godin [54] data that did not fit the Wheeler and Jones measurements. These results confirm our first analysis of the two e.m.f. data (part 3.1) in which the slight disagreement was attributed to composition uncertainties with an impact on the slope values. The perfect agreement between e.m.f. data of Markin and Bones [53] with the flow method determinations of Wheeler and Jones [51] justifies a posteriori our composition uncertainty analysis. We observed also, – either by comparison of Wheeler and Jones [51] data as shown in Fig. 21 or with other studies performed by Markin et al. [47] as shown in Fig. 22, that the isopiestic method with a known oxide as reference (Cr_2O_3 or NbO) is neither in agreement with other studies, even when the same composition analysis method is used. We believe that the determinations with the isopiestic method suffer from an unidentified cause of error and we discard these data. In the range $2 < O/U < 2.005$, the agreement between Markin and Bones [53] and Wheeler and Jones [51] leads directly to the retained array data.

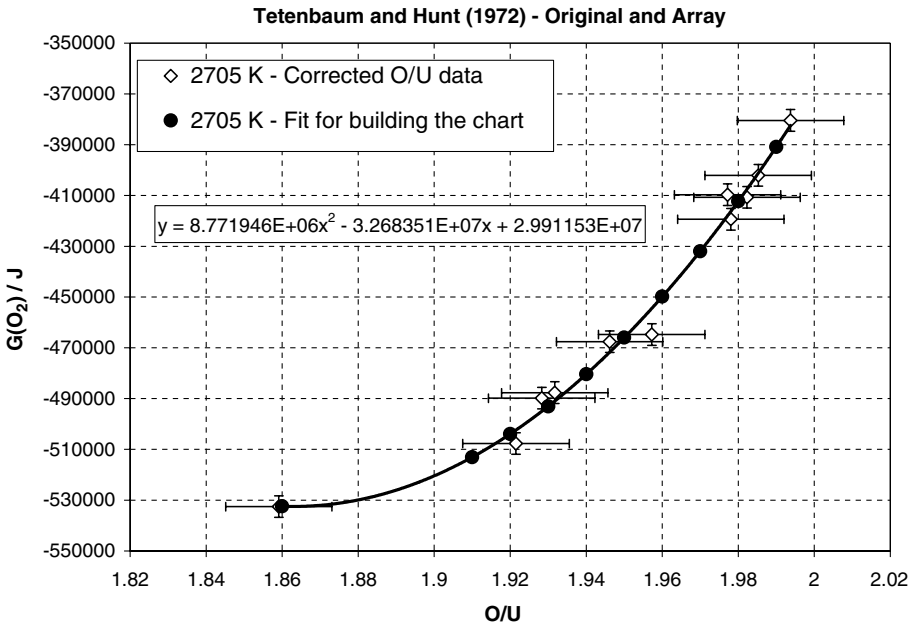

Fig. 19. Example of fit and retained data (black circle) when building the array from Tetenbaum and Hunt [48] original determination at 2705 K. The retained data correspond to 0.01 steps in the O/U values, and their number is generally the same (or less when data are superimposed) as for original data. The uncertainties associated to the array values are those estimated for original values.

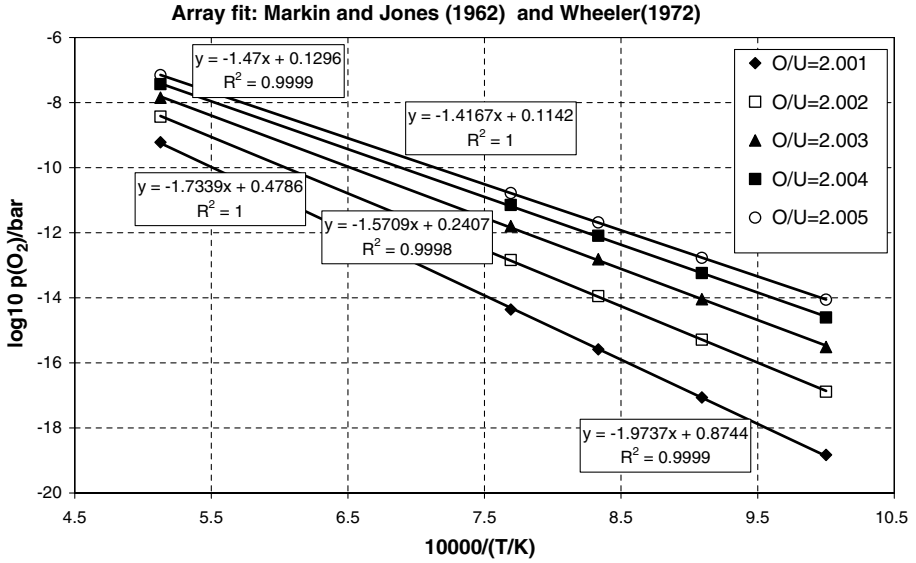

Fig. 20. Comparison array data from e.m.f. determinations of Markin and Bones [53] with higher temperature data of transport method by Wheeler and Jones [51] in the hyperstoichiometric compound UO_{2+x}. The agreement is particularly good as revealed by the correlation coefficient R.

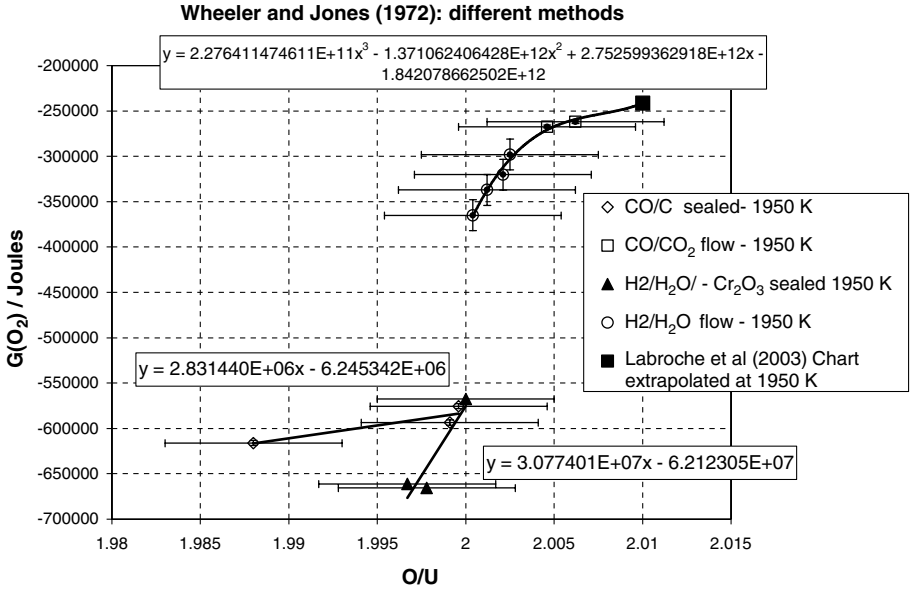

Fig. 21. Intercomparison of the different determinations performed by Wheeler and Jones [51] with different methods and conjunction with preceding array values at O/U = 2.01 from Labroche et al. [3]. As in other studies by Markin et al. [47], the isopiestic method with the Cr_2O_3–Cr or NbO–Nb oxides/metal diphasic references disagreed with other transport or heterogeneous equilibria methods.

In the range $1.98 < O/U < 2.0$, the data of all authors as fitted to produce the array data, for the logarithm of $O_2(g)$ pressures, are compared as shown for instance in Figs. 22 and 23. The agreement is very good between mass spectrometric data of Pattoret et al. [59–62] and flow data of Wheeler and Jones [51]. For these two studies, we note that their composition analysis (polarography and CO/CO_2:10/1 equilibrium) avoids the major uncertainties associated with UO_2 calcination into non-stoichiometric U_3O_{8-z}. Tetenbaum and Hunt [48], although showing a trend with temperature

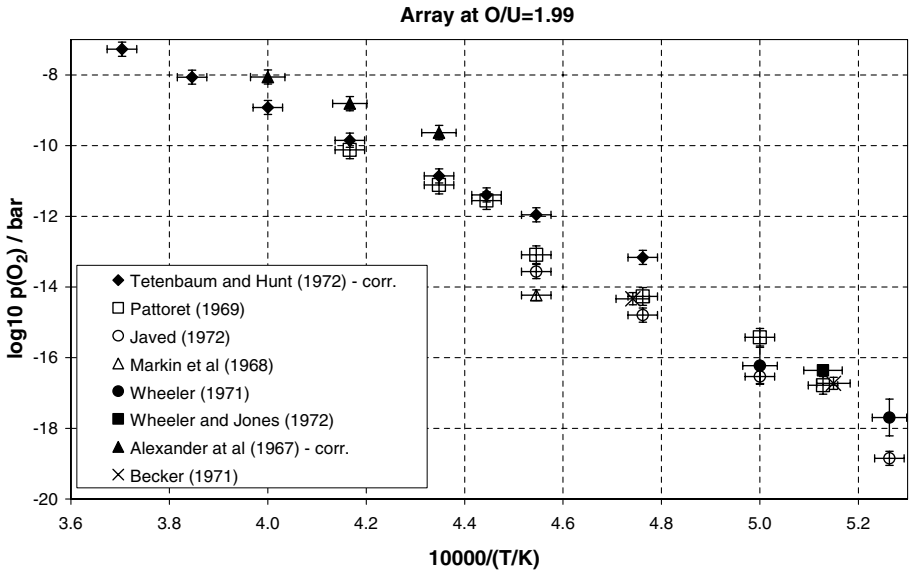

Fig. 22. Decimal logarithm of the O_2 partial pressure array data built to intercompare different works for O/U = 1.99. In this figure, the uncertainties associated to pressure and temperature are quoted and let show that generally these works do not agree each other. In fact, the agreement – when it occurs – is analysed in conjunction with composition for which the uncertainties are more important as shown for instance in Figs. 22, 20, 19, 18... displaying $\bar{G}(O_2)$ as a function of O/U composition. In the present figure, isopiestic method by Markin et al. [47] and transport methods by Alexander et al. [46] and Javed [52] clearly disagreed with the group of authors Tetenbaum and Hunt [48], Pattoret and coworkers [59–62], Wheeler and Jones [51] and Wheeler [50].

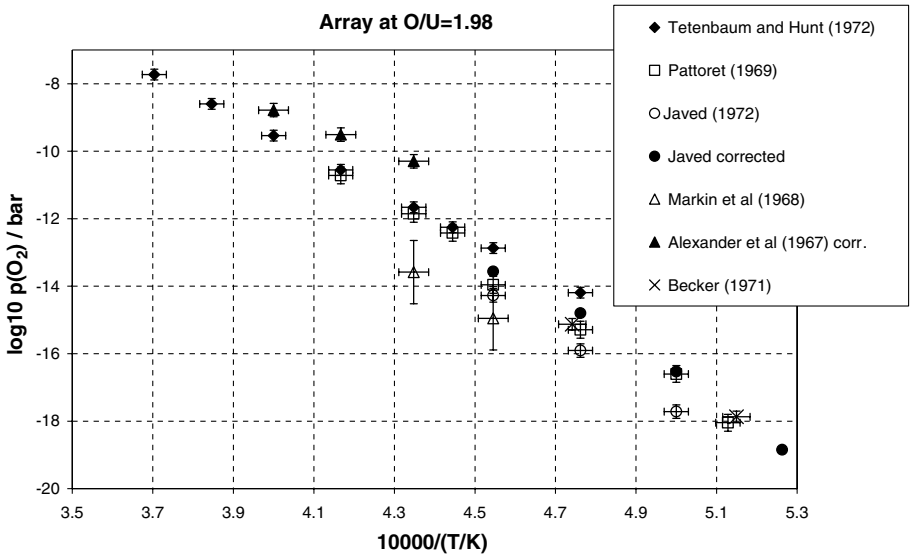

Fig. 23. Same as Fig. 22 for O/U = 1.98.

relatively to the above authors are yet considered as consistent. The observed trend in the comparison may come from composition uncertainty as proposed by Storms [63] although the retained values have been corrected for incomplete oxidation into U_3O_8. In fact, Figs. 22 and 23 cannot display the O/U uncertainties, but in building the primary array data, these uncertainties showed a constant overlap between Tetenbaum and Hunt values and Pattoret's mass spectrometric data for O/U values down to 1.91 as discussed in part 3 and shown for instance in Fig. 24. Conversely, Figs. 22–24 show a constant

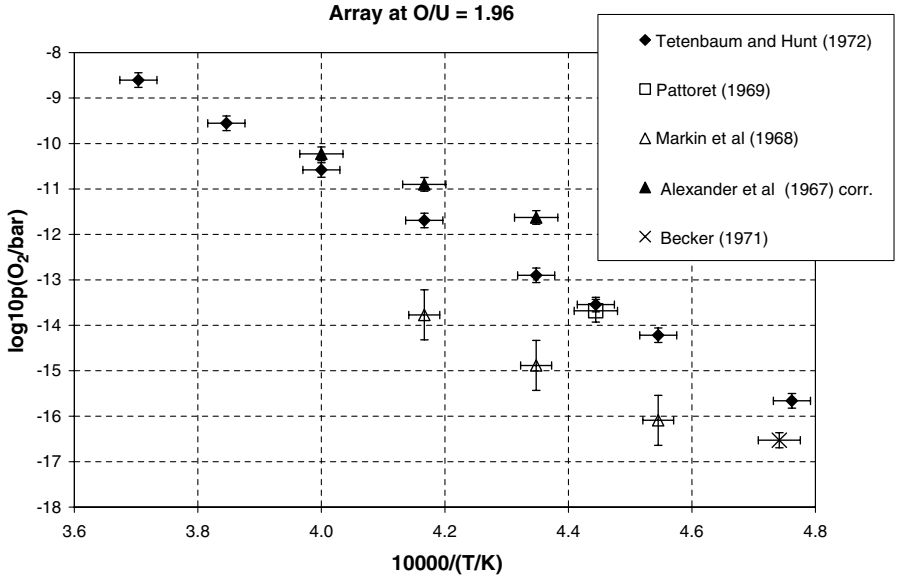

Fig. 24. Same as Fig. 22 for O/U = 1.96.

and large disagreement of the preceding group of authors with studies of Markin et al. [47] and Javed [52]. As already discussed for Wheeler and Jones, the isopiestic method of Markin et al. is probably in error due to the same unidentified cause, although we evaluated a large uncertainty for $\overline{G}(O_2)$, in relation to knowledge of the composition. For the data of Javed, obtained with the H_2/H_2O flow method, it does not seem possible to attribute any large uncertainty to $\overline{G}(O_2)$, and we believe that the composition uncertainty is not well evaluated in the calcination procedure. Indeed, the author observed some trends in the calcination analyses with a 'critical' temperature at 1123 K. Taking into account the shape of these Gibbs energy results that shows a sharp curvature very close to O/U = 2, our assumption is that the composition analysis and its uncertainty may present an abnormal trend as a function of the analysed composition. Finally we do not retain the data of Javed [52] and Markin et al. [47]. Similar large discrepancies were observed for Aitkin et al. [45], Alexander [46] (as shown for instance in Fig. 22) and these data were not retained.

Finally, the retained Gibbs energy data for oxygen in their equivalent array values, as well as their original associated uncertainties are presented in Appendix A, Table A.1. Gibbs energy data for uranium of Pattoret et al. [59–62] and Storms [63] are in agreement and retained as a array as presented in Appendix A, Table A.2.

5. Partial oxygen mixing enthalpies

This thermodynamic property can be obtained first by derivation of partial Gibbs energies of oxygen either from direct experimental values of each author or from our array values, and second from direct calorimetric measurements as carried out by Gerdanian and Dodé [84]. In these experiments, a series of UO_2 samples, rings separated by alumina ring spacers, are oxidized by introduction of small O_2(g) quantities in a Calvet calorimeter, starting from O/U $\cong$ 2 up to O/U = 2.02. The heat of reaction reported for the quantity of O_2 leads directly to the partial enthalpy of mixing of oxygen in the UO_{2+x} compound with the assumption of complete and rapid enough (20 mn in these experiments) reaction. Results of the two methods – derivation and calorimetric – are presented in Fig. 25. For the derivation method, we use our array of selected data in order to increase the accuracy, and close to O/U = 2 some complementary original data of Markin and Bones [53], other values of this study being selected in the present array. The junction with the preceding selected values of the Labroche et al. [3] array shows agreement between the two arrays, meanwhile the calorimetric values agree only at O/U = 2.02, mainly because the $\overline{H}(O_2)$ for O/U = 2.02 has been chosen in calorimetry as a calibration reference, but yet we have to quote that the original calorimetric value at O/U = 2.02 was included in the uncertainty range of other works.

Table A.1
Array of retained partial Gibbs energies of oxygen and related uncertainties for the monophasic UO_{2-x}–$UO_{2+\varepsilon}$ domain

Authors (date) Ref.	O/U	d(O/U)	T/K	dT/K	$G(O_2)$/J	d$G(O_2)$/J	$\log 10\,p(O_2)$ (bar)	(dp/p)	10 000/T/K	d(10 000/T)/K
Baichi U+UO_2 diphasic	1.8	0.0001	2000	15	−741 739	−7417	−19.372	0.19	5.000	0.038
	1.8	0.0001	2050	15	−733 651	−7337	−18.693	0.19	4.878	0.036
	1.8	0.0001	2100	15	−725 991	−7260	−18.058	0.18	4.762	0.034
	1.8	0.0001	2150	15	−718 762	−7188	−17.462	0.17	4.651	0.032
	1.8	0.0001	2200	15	−711 962	−7120	−16.904	0.17	4.545	0.031
	1.8	0.0001	2250	15	−705 591	−7056	−16.380	0.16	4.444	0.030
Tetenbaum and Hunt	1.9	0.0144	2400	15	−627 511	6275	−13.657	0.14	4.167	0.026
	1.9	0.0144	2500	15	−598 360	5984	−12.502	0.13	4.000	0.024
	1.9	0.0144	2600	15	−569 209	5692	−11.435	0.11	3.846	0.022
	1.9	0.0144	2700	15	−540 058	5401	−10.448	0.10	3.704	0.021
Tetenbaum and Hunt	1.91	0.0144	2200	15	−694 172	6942	−16.481	0.16	4.545	0.031
	1.91	0.0144	2400	15	−623 990	6240	−13.580	0.14	4.167	0.026
	1.91	0.0144	2500	15	−588 900	5889	−12.304	0.12	4.000	0.024
	1.91	0.0144	2600	15	−553 809	5538	−11.126	0.11	3.846	0.022
	1.91	0.0144	2700	15	−518 718	5187	−10.035	0.10	3.704	0.021
Pattoret	1.91	0.0077	2250	15	−660 851	6609	−15.342	0.15	4.444	0.030
Tetenbaum and Hunt	1.92	0.0144	2200	15	−656 079	6561	−15.577	0.16	4.545	0.031
	1.92	0.0144	2400	15	−600 567	6006	−13.071	0.13	4.167	0.026
	1.92	0.0144	2500	15	−572 812	5728	−11.968	0.12	4.000	0.024
	1.92	0.0144	2600	15	−545 056	5451	−10.950	0.11	3.846	0.022
	1.92	0.0144	2700	15	−517 300	5173	−10.008	0.10	3.704	0.021
Pattoret	1.92	0.0077	2250	15	−650 522	6505	−15.102	0.15	4.444	0.030
Tetenbaum and Hunt	1.93	0.0144	2200	15	−644 407	6444	−15.300	0.15	4.545	0.031
	1.93	0.0144	2250	15	−630 269	6303	−14.632	0.15	4.444	0.030
	1.93	0.0144	2300	15	−616 131	6161	−13.992	0.14	4.348	0.028
	1.93	0.0144	2400	15	−587 854	5879	−12.794	0.13	4.167	0.026
	1.93	0.0144	2500	15	−559 578	5596	−11.691	0.12	4.000	0.024
	1.93	0.0144	2600	15	−531 302	5313	−10.674	0.11	3.846	0.022
	1.93	0.0144	2700	15	−503 025	5030	−9.731	0.10	3.704	0.021
Pattoret	1.93	0.0077	2250	15	−638 871	6389	−14.831	0.15	4.444	0.030
Tetenbaum and Hunt	1.94	0.0144	2100	15	−657 078	6571	−16.344	0.16	4.762	0.034
	1.94	0.0144	2200	15	−628 947	6289	−14.933	0.15	4.545	0.031
	1.94	0.0144	2250	15	−614 882	6149	−14.274	0.14	4.444	0.030
	1.94	0.0144	2300	15	−600 816	6008	−13.645	0.14	4.348	0.028
	1.94	0.0144	2400	15	−572 686	5727	−12.464	0.12	4.167	0.026
	1.94	0.0144	2500	15	−544 555	5446	−11.378	0.11	4.000	0.024
	1.94	0.0144	2600	15	−516 424	5164	−10.375	0.10	3.846	0.022
	1.94	0.0144	2700	15	−488 294	4883	−9.446	0.09	3.704	0.021
Pattoret	1.94	0.0077	2250	15	−625 305	6253	−14.516	0.15	4.444	0.030
Tetenbaum and Hunt	1.95	0.0144	2100	15	−647 275	6473	−16.100	0.16	4.762	0.034
	1.95	0.0144	2200	15	−617 190	6172	−14.654	0.15	4.545	0.031
	1.95	0.0144	2250	15	−602 147	6021	−13.979	0.14	4.444	0.030
	1.95	0.0144	2300	15	−587 104	5871	−13.333	0.13	4.348	0.028
	1.95	0.0144	2400	15	−557 019	5570	−12.123	0.12	4.167	0.026
	1.95	0.0144	2500	15	−526 933	5269	−11.009	0.11	4.000	0.024
	1.95	0.0144	2600	15	−496 848	4968	−9.982	0.10	3.846	0.022
	1.95	0.0144	2700	15	−466 762	4668	−9.030	0.09	3.704	0.021
Pattoret	1.95	0.0077	2250	15	−609 086	6091	−14.140	0.14	4.444	0.030

Table A.1 (*continued*)

Authors (date) Ref.	O/U	d(O/U)	T/K	dT/K	$G(O_2)$/J	d$G(O_2)$/J	$\log 10\,p(O_2)$ (bar)	(dp/p)	10000/T/K	d(10000/T)/K
Tetenbaum and Hunt	1.96	0.0144	2100	15	−629631	6296	−15.661	0.16	4.762	0.034
	1.96	0.0144	2200	15	−598825	5988	−14.218	0.14	4.545	0.031
	1.96	0.0144	2250	15	−583422	5834	−13.544	0.14	4.444	0.030
	1.96	0.0144	2300	15	−568020	5680	−12.900	0.13	4.348	0.028
	1.96	0.0144	2400	15	−537214	5372	−11.692	0.12	4.167	0.026
	1.96	0.0144	2500	15	−506408	5064	−10581	0.11	4.000	0.024
	1.96	0.0144	2600	15	−475603	4756	−9.555	0.10	3.846	0.022
	1.96	0.0144	2700	15	−444797	4448	−8.605	0.09	3.704	0.021
Pattoret	1.96	0.0077	2250	15	−589331	5893	−13.681	0.14	4.444	0.030
Becker	1.96	0.0054	2109	15	−667320	6673	−16.527	0.17	4.742	0.034
Tetenbaum and Hunt	1.97	0.0144	2100	15	−604025	6040	−15.024	0.15	4.762	0.034
	1.97	0.0144	2200	15	−573734	5737	−13.622	0.14	4.545	0.031
	1.97	0.0144	2250	15	−558589	5586	−12.968	0.13	4.444	0.030
	1.97	0.0144	2300	15	−543443	5434	−12.342	0.12	4.348	0.028
	1.97	0.0144	2400	15	−513153	5132	−11.168	0.11	4.167	0.026
	1.97	0.0144	2500	15	−482862	4829	−10.089	0.10	4.000	0.024
	1.97	0.0144	2600	15	−452572	4526	−9.092	0.09	3.846	0.022
	1.97	0.0144	2700	15	−422281	4223	−8.169	0.08	3.704	0.021
Pattoret	1.97	0.0077	2250	15	−565015	5650	−13.117	0.13	4.444	0.030
	1.97	0.0077	1950	15	−671579	9200	−17.989	0.25	5.128	0.039
	1.97	0.0077	2000	15	−635408	9200	−16.595	0.24	5.000	0.038
	1.97	0.0077	2100	15	−613279	9200	−15.254	0.23	4.762	0.034
	1.97	0.0077	2200	15	−589869	9200	−14.005	0.22	4.545	0.031
	1.97	0.0077	2300	15	−527650	9200	−11.983	0.21	4.348	0.028
	1.97	0.0077	2400	15	−506043	9200	−11.013	0.20	4.167	0.026
Becker	1.97	0.0054	2109	15	−640351	6404	−15.860	0.16	4.742	0.034
Tetenbaum and Hunt	1.98	0.0144	2100	15	−570576	5706	−14.192	0.14	4.762	0.034
	1.98	0.0144	2200	15	−542036	5420	−12.869	0.13	4.545	0.031
	1.98	0.0144	2250	15	−527765	5278	−12.252	0.12	4.444	0.030
	1.98	0.0144	2300	15	−513495	5135	−11.662	0.12	4.348	0.028
	1.98	0.0144	2400	15	−484954	4850	−10.554	0.11	4.167	0.026
	1.98	0.0144	2500	15	−456413	4564	−9.536	0.10	4.000	0.024
	1.98	0.0144	2600	15	−427872	4279	−8.596	0.09	3.846	0.022
	1.98	0.0144	2700	15	−399331	3993	−7.725	0.08	3.704	0.021
Pattoret	1.98	0.0077	2250	15	−534968	5350	−12.419	0.12	4.444	0.030
	1.98	0.0077	1950	15	−673724	9200	−18.047	0.25	5.128	0.039
	1.98	0.0077	2000	15	−635648	9200	−16.601	0.24	5.000	0.038
	1.98	0.0077	2100	15	−614724	9200	−15.290	0.23	4.762	0.034
	1.98	0.0077	2200	15	−587964	9200	−13.960	0.22	4.545	0.031
	1.98	0.0077	2300	15	−522000	9200	−11.855	0.21	4.348	0.028
	1.98	0.0077	2400	15	−492370	9200	−10.716	0.20	4.167	0.026
Becker	1.98	0.0054	2109	15	−610819	6108	−15.128	0.15	4.742	0.034
	1.98	0.0054	1942	15	−664370	6644	−17.869	0.18	5.149	0.040
Tetenbaum and Hunt	1.99	0.0144	2100	15	−529245	5292	−13.164	0.13	4.762	0.034
	1.99	0.0144	2200	15	−503689	5037	−11.959	0.12	4.545	0.031
	1.99	0.0144	2250	15	−490911	4909	−11.396	0.11	4.444	0.030
	1.99	0.0144	2300	15	−478133	4781	−10.858	0.11	4.348	0.028
	1.99	0.0144	2400	15	−452577	4526	−9.850	0.10	4.167	0.026
	1.99	0.0144	2500	15	−427021	4270	−8.922	0.09	4.000	0.024
	1.99	0.0144	2600	15	−401465	4015	−8.065	0.08	3.846	0.022
	1.99	0.0144	2700	15	−375909	3759	−7.272	0.07	3.704	0.021

(*continued on next page*)

Table A.1 (*continued*)

Authors (date) Ref.	O/U	d(O/U)	T/K	dT/K	$G(O_2)$/J	d$G(O_2)$/J	$\log 10\,p(O_2)$ (bar)	(dp/p)	10000/T/K	d(10000/T)/K
Pattoret	1.99	0.0077	2250	15	−497876	4979	−11.558	0.12	4.444	0.030
	1.99	0.0077	1950	15	−626531	9200	−16.782	0.25	5.128	0.039
	1.99	0.0077	2000	15	−590512	9200	−15.422	0.24	5.000	0.038
	1.99	0.0077	2100	15	−573631	9200	−14.268	0.23	4.762	0.034
	1.99	0.0077	2200	15	−551341	9200	−13.090	0.22	4.545	0.031
	1.99	0.0077	2300	15	−489450	9200	−11.115	0.21	4.348	0.028
	1.99	0.0077	2400	15	−465023	9200	−10.121	0.20	4.167	0.026
Becker	1.99	0.0054	2109	15	−578723	5787	−14.333	0.14	4.742	0.034
	1.99	0.0054	1942	15	−621866	6219	−16.726	0.17	5.149	0.040
Wheeler	1.99	0.005	1800	15	−665806	20000	−19.321	0.58	5.556	0.046
	1.99	0.005	1900	15	−643623	20000	−17.694	0.55	5.263	0.042
	1.99	0.005	2000	15	−621440	20000	−16.230	0.52	5.000	0.038
Wheeler and Jones	1.99	0.005	1950	15	−610776	6108	−16.360	0.16	5.128	0.039
Pattoret	2	0.0077	2250	15	−452279	4523	−10.500	0.10	4.444	0.030
	2	0.0077	2100	15	−490000	9200	−12.188	0.23	4.762	0.034
	2	0.0077	2200	15	−480000	9200	−11.396	0.22	4.545	0.031
	2	0.0077	2300	15	−430000	9200	−9.765	0.21	4.348	0.028
Becker	2	0.0054	1942	15	−568608	5686	−15.294	0.15	5.149	0.040
Wheeler	2	0.005	1800	15	−634932	20000	−18.425	0.58	5.556	0.046
	2	0.005	1900	15	−615946	20000	−16.933	0.55	5.263	0.042
	2	0.005	2000	15	−596960	20000	−15.591	0.52	5.000	0.038
Wheeler and Jones	2	0.005	1950	15	−582462	5825	−15.602	0.16	5.128	0.039
	2	0.005	1950	15	−575030	5750	−15.403	0.15	5.128	0.039
Markin	2.0005	0.00013	1000	5	−383865	3839	−20.051	0.20	10.000	0.050
		0.00013	1100	5	−382994	3830	−18.186	0.18	9.091	0.041
		0.00013	1200	5	−381955	3820	−16.626	0.17	8.333	0.035
		0.00013	1300	5	−381471	3815	−15.327	0.15	7.692	0.030
Markin	2.001	0.00013	1000	5	−360506	3605	−18.830	0.19	10.000	0.050
		0.00013	1100	5	−359343	3593	−17.063	0.17	9.091	0.041
		0.00013	1200	5	−358060	3581	−15.586	0.16	8.333	0.035
		0.00013	1300	5	−357370	3574	−14.359	0.14	7.692	0.030
Wheeler		0.005	1950	15	−344170	3442	−9.219	0.09	5.128	0.039
Markin	2.002	0.00013	1000	5	−323266	3233	−16.885	0.17	10.000	0.050
		0.00013	1100	5	−321876	3219	−15.284	0.15	9.091	0.041
		0.00013	1200	5	−320404	3204	−13.946	0.14	8.333	0.035
		0.00013	1300	5	−319554	3196	−12.840	0.13	7.692	0.030
Wheeler		0.005	1950	15	−314717	3147	−8.430	0.08	5.128	0.039
Markin	2.003	0.00013	1000	5	−296972	2970	−15.512	0.16	10.000	0.050
		0.00013	1100	5	−295738	2957	−14.043	0.14	9.091	0.041
		0.00013	1200	5	−294396	2944	−12.814	0.13	8.333	0.035
		0.00013	1300	5	−293657	2937	−11.799	0.12	7.692	0.030
Wheeler		0.005	1950	15	−292962	2930	−7.847	0.08	5.128	0.039
Markin	2.004	0.00013	1000	5	−279601	2796	−14.604	0.15	10.000	0.050
		0.00013	1100	5	−278790	2788	−13.238	0.13	9.091	0.041
		0.00013	1200	5	−277801	2778	−12.092	0.12	8.333	0.035
		0.00013	1300	5	−277360	2774	−11.144	0.11	7.692	0.030
Wheeler		0.005	1950	15	−277542	2775	−7.434	0.07	5.128	0.039

Table A.1 (*continued*)

Authors (date) Ref.	O/U	d(O/U)	T/K	dT/K	$G(O_2)$/J	d$G(O_2)$/J	$\log 10\, p(O_2)$ (bar)	(dp/p)	10000/T/K	d(10000/T)/K
Markin	2.005	0.00013	1000	5	−269124	2691	−14.057	0.14	10.000	0.050
		0.00013	1100	5	−268891	2689	−12.768	0.13	9.091	0.041
		0.00013	1200	5	−268383	2684	−11.682	0.12	8.333	0.035
		0.00013	1300	5	−268349	2683	−10.782	0.11	7.692	0.030
Wheeler		0.05	1950	15	−267088	2671	−7.154	0.07	5.128	0.039
Wheeler	2.006	0.05	1950	15	−260237	2602	−6.971	0.07	5.128	0.039
Markin	2.01	0.00013	1000	5	−249271	2493	−13.020	0.13	10.000	0.050
		0.00013	1100	5	−250224	2502	−11.882	0.12	9.091	0.041
		0.00013	1200	5	−250702	2507	−10.913	0.11	8.333	0.035
		0.00013	1300	5	−251506	2515	−10.105	0.10	7.692	0.030

Table A.2
Array of retained partial Gibbs energies of uranium and related uncertainties for the monophasic UO_{2-x}–UO_2 domain (by Baichi and Chatillon)

	T/K	dT	O/U	d(O/U)	G(U)/J	dG(U)/J	log10 a(U)	da(U)/a(U)
Storms [63]	1950	5	1.93	0.0132	−4704	10000	−0.126	0.62
	1950	5	1.94	0.0132	−7852	10000	−0.210	0.62
	1950	5	1.95	0.0132	−18836	10000	−0.505	0.62
	1950	5	1.96	0.0132	−37656	10000	−1.009	0.62
	1950	5	1.97	0.0132	−64311	10000	−1.723	0.62
	1950	5	1.98	0.0132	−98802	10000	−2.647	0.62
	1950	5	1.99	0.0132	−141128	10000	−3.780	0.62
Pattoret [59]	1950	15	1.98	0.0077	−102845	9200	−2.55	0.57
	1950	15	1.99	0.0077	−137155	9200	−3.674	0.57
Storms [63]	2000	5	1.93	0.0132	−9028	10000	−0.236	0.60
	2000	5	1.94	0.0132	−14642	10000	−0.382	0.60
	2000	5	1.95	0.0132	−27197	10000	−0.710	0.60
	2000	5	1.96	0.0132	−46694	10000	−1.220	0.60
	2000	5	1.97	0.0132	−73134	10000	−1.910	0.60
	2000	5	1.98	0.0132	−106515	10000	−2.782	0.60
	2000	5	1.99	0.0132	−146837	10000	−3.835	0.60
Pattoret [59]	2000	15	1.98	0.0077	−104635	9200	−2.733	0.55
	2000	15	1.99	0.0077	−151336	9200	−3.952	0.55
	2000	15	2	0.0077	−238610	9200	−6.232	0.55
Storms [63]	2100	5	1.93	0.0132	−19686	10000	−0.490	0.57
	2100	5	1.94	0.0132	−28266	10000	−0.703	0.57
	2100	5	1.95	0.0132	−43385	10000	−1.079	0.57
	2100	5	1.96	0.0132	−65044	10000	−1.618	0.57
	2100	5	1.97	0.0132	−93243	10000	−2.319	0.57
	2100	5	1.98	0.0132	−127980	10000	−3.183	0.57
	2100	5	1.99	0.0132	−169258	10000	−4.210	0.57
Pattoret [59]	2100	15	1.98	0.0077	−124600	9200	−3.099	0.53
	2100	15	1.99	0.0077	−168073	9200	−4.180	0.53
	2100	15	2	0.0077	−249708	9200	−6.211	0.53
Storms [63]	2200	5	1.93	0.0132	−30162	10000	−0.716	0.55
	2200	5	1.94	0.0132	−42169	10000	−1.001	0.55
	2200	5	1.95	0.0132	−60121	10000	−1.427	0.55
	2200	5	1.96	0.0132	−84018	10000	−1.995	0.55
	2200	5	1.97	0.0132	−113860	10000	−2.703	0.55
	2200	5	1.98	0.0132	−149647	10000	−3.553	0.55
	2200	5	1.99	0.0132	−191378	10000	−4.544	0.55

(*continued on next page*)

Table A.2 (*continued*)

	T/K	dT	O/U	d(O/U)	*G*(U)/J	d*G*(U)/J	log10 *a*(U)	d*a*(U)/*a*(U)
Pattoret [59]	2200	15	1.98	0.0077	−124 570	9200	−2.958	0.50
	2200	15	1.99	0.0077	−168 043	9200	−3.990	0.50
	2200	15	2	0.0077	−249 678	9200	−5.928	0.50
Pattoret [59] isothermal run	2250	15	1.85	0.0200	0	5200	0.000	0.28 phase limit
	2250	15	1.91	0.0077	−45 036	5200	−1.046	0.28
	2250	15	1.92	0.0077	−53 970	5200	−1.253	0.28
	2250	15	1.93	0.0077	−64 254	5200	−1.492	0.28
	2250	15	1.94	0.0077	−76 583	5200	−1.778	0.28
	2250	15	1.95	0.0077	−91 797	5200	−2.131	0.28
	2250	15	1.96	0.0077	−110 889	5200	−2.574	0.28
	2250	15	1.97	0.0077	−135 000	5200	−3.134	0.28
	2250	15	1.98	0.0077	−165 423	5200	−3.840	0.28
	2250	15	1.99	0.0077	−203 598	5200	−4.726	0.28
	2250	15	2	0.0077	−251 115	5200	−5.830	0.28
Pattoret [59]	2300	15	1.97	0.0077	−150 554	9200	−3.419	0.48
	2300	15	1.98	0.0077	−169 725	9200	−3.854	0.48
	2300	15	1.99	0.0077	−203 330	9200	−4.618	0.48
	2300	15	2	0.0077	−251 367	9200	−5.709	0.48
Pattoret [59]	2400	15	1.98	0.0077	−192 378	9200	−4.187	0.46
	2400	15	1.99	0.0077	−221 776	9200	−4.827	0.46
	2400	15	2	0.0077	−254 778	9200	−5.545	0.46

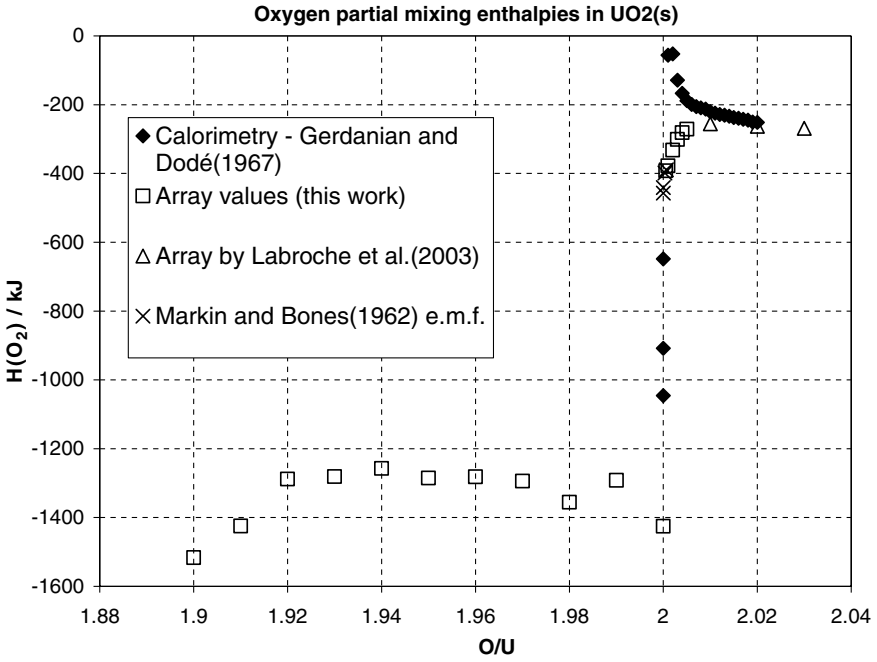

Fig. 25. Partial enthalpy of mixing for oxygen measured directly by calorimetry [84] and comparison with values derived from partial Gibbs energies as retained in this work (array values), in the preceding array by Labroche et al. [3], and from Markin and Bones [53] e.m.f. determinations at stoichiometry.

However, we observe that calorimetric values disagree largely for slightly hyperstoichiometric compounds, and let suppose the presence of a pronounced peak at about O/U = 2.0015–2.0018, meanwhile the derivation method would have a slight maximum around O/U ≅ 2.01.

The pronounced peak in calorimetry could come from unreacted oxygen or kinetic problems as discussed by Gerdanian and Dodé [84] and summarized by Gerdanian [85]. Gerdanian and Dodé attempted to evaluate the impact of these features by different techniques, – resistivity measurements, use of sintered, oxidized U or melted samples, or by estimations of diffusion in the bulk or at the grain boundaries. The conclusions from their studies are not clear, but we observe some anomalous features that demonstrate non-equilibrium behaviour; for example:

- the O_2 input quantities were always larger, – as stated by the authors, than the oxygen increase analysed in the samples,
- an oxygen gradient was observed along the column of piled rings,
- resistivity measurements showed first a rapid reaction, 20 mn, as in the calorimeter, and then a very slow reaction during 6 days. The heat associated to this second reaction could not be detected by the calorimeter,
- homogenisation (partly or fully) of the samples was observed when stopping the calorimeter overnight, whatever are the atmospheric conditions, including vacuum. Restarting the experiments overnight always led to first heat effects larger than that those observed at the preceding step. This feature indicates not only a reducing effect of the surface layer as postulated by Gerdanian and Dodé, but also probably a further and low speed consumption of O_2 during the night since the registered curves could be matched by simple O/U compositional translation.

All these features let suppose the peak observed in calorimetry to be closely related to incomplete reaction. We believe that the diffusion of oxygen at, or close to, the stoichiometry is more complex than analysed by Gerdanian and Dodé in terms of bulk or grain boundary diffusion: probably due to the change in the defects nature near the stoichiometric composition, diffusion occurs at least according to two different regimes than can lead to a protective layer and share the material in at least two different zones.

In conclusion, we do not retain the calorimetric values that are in complete disagreement with our Gibbs energy retained array value and were probably in error due to kinetic limitations in the analysed composition range.

6. Conclusion

The present analysis was undertaken in order to identify the origin of large discrepancies existing in partial Gibbs energies of oxygen in the non-stoichiometric domain of the UO_{2-x} compound. Indeed, this property remains an important data set in view of modelling the thermodynamic behaviour of the UO_2 compound and its fission products. The final analysis of original data was performed mainly by intercomparison of activity or oxygen pressure array data because it is this property, which is directly measured. Thus the uncertainty analysis, closely related to the measurement techniques is clearly more pertinent than the Gibbs energy values themself. We first observe that, for the major part of the studies, the Gibbs energy uncertainties cannot explain the discrepancies in the results as published.

These discrepancies, – due to the steep gradient of oxygen potential (and correlated uranium potential) in the $UO_{2\pm x}$ compound – are mainly attributed to chemical analysis of composition as already suggested by Pattoret [59] and Storms [63]. From the first analysis of the causes of uncertainty by Labroche et al. [3] attributed to the calcination process of UO_2 into non-stoichiometric U_3O_8, we observe that the major disagreement between

Table 7
Evolution of the decimal logarithm of O_2 partial pressures (in bar) as a function of the inverse of temperature ($\log_{10} p_{O_2} = A/T$ (K) + B) in the UO_{2-x}–$UO_{2.00}$ monophasic domain for different compositions ($2-x$ to $2+x$) according to our treatment of experimental selected data with constant intervals of a (T, x) array

O/U = (2 − x) composition	A	B	Temperature range (K)
1.90	−79208	19.025	2400–2700
1.91	−74821	17.596	2200–2700
1.92	−63481	13.216	2200–2700
1.93	−66370	14.748	2200–2700
1.94	−63674	13.860	2200–2700
1.95	−65838	15.143	2200–2700
1.96	−65727	15.520	2200–2700
1.97	−61126	13.913	2100–2700
1.98	−66300	16.681	2000–2700
1.99	−66439	17.578	1800–2700
2.00	−69245	19.808	1800–2250
2.001	−19737	0.8744	1000–1950
2.002	−17339	0.4786	1000–1950
2.003	−15709	0.2407	1000–1950
2.004	−14700	0.1296	1000–1950
2.005	−14167	0.1142	1000–1950

Original array values are presented in Appendix A.

Table 8
Comparison of our oxygen pressures as deduced from our array with those coming from Lindemer and Besmann [86] compilation

Temperature (K)	Composition (O/U)	p_{O_2} [86] (bar)	p_{O_2} this work (bar)	Relative difference (%) (p_{O_2}) [86] $-p_{O_2}$ [this work]/p_{O_2} [this work]
2250	1.90	1.71×10^{-16}	6.62×10^{-17}	158
	1.97	5.61×10^{-15}	5.57×10^{-14}	−90
	1.99	1.34×10^{-13}	1.12×10^{-12}	−88
	2.00	3.44×10^{-10}	1.08×10^{-11}	308
1500	2.001	7.31×10^{-13}	5.20×10^{-13}	41
	2.003	5.33×10^{-12}	5.86×10^{-11}	−91

The comparison is done for those compositions that match with our array.

studies is derived from those which used this method of analysis. We tentatively try to correct those studies with a relation proposed by Labroche et al. [3] on the basis of the Ackermann and Chang data [68]. Other methods for composition analysis, such as polarography and CO/CO_2:10/1 equilibration, lead to results in agreement and thus were generally retained. We encourage greatly some revised procedure to be established for future works when using calcination method, as for instance use of flowing pure oxygen and a final oxidizing cycle at lower than 873 K to recover completely the U_3O_8 stoichiometry.

The present analysed data, and their retained values are displayed as a $\{G(O_2), O/U, T\}$ array from which two main calculations may be performed in order to improve the thermodynamic description of the UO_2 non-stoichiometric phase:

- Firstly a least square fit of each array nod (the slope of $\Delta G(O_2)$ – temperature line) or series at constant composition,
- Secondly, the use of the array values in an optimisation procedure including the original uncertainties as weighting factors.

The least square fitting procedure leads to a series of pressure relations as presented in Table 7, that can be compared to the original work of Lindemer and Bessman [86] for some similar compositions. Observed large and significant differences are mainly derived from our composition scale that have been modified for studies using the calcination method. Our second result is a better definition of the uncertainty limits, although large extrapolations (some 500 K) to the solidus may be questionable as can be achieved with Table 7. For this reason our opinion is that an optimisation procedure taking into account the phase diagram data will allow a better thermodynamic description of the $UO_{2\pm x}$ compound.

A future refinement of our original optimisation by Guéneau et al. [87] is now rendered necessary since the present array is improved when compared with the preceding one [38] mainly for compositions close to the stoichiometric one. We have to keep in mind that the shape of the Gibbs partial energies in this domain is determinant in the modelling of thermodynamic properties of the $UO_{2\pm x}$ domain. The present critical analysis was undertaken as an independent and important primary step in order to circumvent the usual difficulties encountered in optimisation procedures, as illustrated in the studies of Fisher and Chevalier [88]. Fisher and Chevalier have used an arbitrary set of original experimental data [52] to optimise a given lattice model of the UO_{2-x} phase. Such an approach is not justified until a complete critical assessment of the published phase diagram and thermodynamic data has been undertaken and appropriate weighting factors and uncertainties have been included.

The present work is a necessary step before optimisation, especially for systems in which much data are available: it is the only means to prepare an acceptable and reliable thermodynamic description of such chemical systems with significant non-stoichiometric domains.

Acknowledgements

The authors acknowledge Electricité De France for sponsoring this study in the framework of research program on severe nuclear accidents, and Dr Paul Potter for help in the preparation of the final text.

Appendix A

Array values for the partial Gibbs energy of mixing of uranium and oxygen in the monaphasic $UO_{2\pm x}$ non-stoichiometric compound proposed for optimization of thermodyamic and phase diagram data in the U–O system with the retained corresponding authors.

References

[1] J.M. Seiler, K. Froment, Multiphase Sci. Technol. 12 (2000) 117.
[2] M. Baïchi, C. Chatillon, G. Ducros, K. Froment, J. Nucl. Mater., in press, doi:10.1016/j.jnucmat.2005.10.001.
[3] D. Labroche, O. Dugne, C. Chatillon, J. Nucl. Mater. 312 (2003) 21.
[4] D. Labroche, O. Dugne, C. Chatillon, J. Nucl. Mater. 312 (2003) 50.
[5] B. Jansson, Report TRITE-MAC-0234, April 1984, Royal Institute Technology, S10044 Stockholm 70, Sweden.
[6] M.H. Rand, R.J. Ackermann, F. Gronvold, F.L. Oetting, A. Pattoret, Rev. Int. Hautes Temper. Refract. Fr. 15 (1978) 355.
[7] M.A. Bredig, High Temperature Thermochemistry: the order–disorder (γ) transition in uranium dioxide and other solids of the fluorite type. Effect of ion size and deviation from stoichiometry, Report ORNL-4437, 1969, 10 p.
[8] R. Szwarc, J. Phys. Chem. Solids 30 (1969) 705.
[9] J.F. Kerrisk, D.G. Clifton, Nucl. Technol. 16 (1972) 531.
[10] D.A. MacInnes, J. Nucl. Mater. 78 (1978) 225.
[11] D.A. MacInnes, C.R.A. Catlow, J. Nucl. Mater. 89 (1980) 354.
[12] J.H. Harding, P. Masri, A.M. Stoncham, J. Nucl. Mater. 92 (1980) 73.
[13] K.A. Long, J.F. Babelot, J. Magill, R.W. Ohse, High Temp. High Press. 12 (1980) 515.
[14] J.K. Fink, M.G. Chasanov, L. Leibowitz, J. Nucl. Mater. 102 (1981) 17.
[15] J.K. Fink, Int. J. Thermophys. 3 (1982) 165.
[16] P. Browning, G.J. Hyland, J. Ralph, High Temp. High Press. 15 (1983) 169.
[17] M.H. Rand, Pure Appl. Chem. 56 (1984) 1545.
[18] M. Hoch, J. Nucl. Mater. 130 (1985) 94.
[19] G.J. Hyland, R.W. Ohse, J. Nucl. Mater. 140 (1986) 149.
[20] Shian Peng, Göran Grimvall, J. Nucl. Mater. 210 (1994) 115.
[21] J.K. Fink, J. Nucl. Mater. 279 (2000) 1.
[22] C. Affortit, High Temp. High Press. 1 (1969) 27.
[23] C. Affortit, J.P. Marcon, Rev. Int. Hautes Tempér. Réfract. 7 (1970) 236.
[24] J.P. Hiernaut, C. Ronchi, High Temp. High Press. 21 (1979) 119.
[25] J.P. Hiernaut, G.J. Hyland, C. Ronchi, Int. J. Thermophys. 14 (1993) 259.
[26] C. Ronchi, J.P. Hiernaut, R. Selfslog, Nucl. Sci. Eng. 113 (1993) 1.
[27] C. Ronchi, G.J. Hyland, J. Alloys Compd. 213/214 (1994) 159.
[28] D. Halton, J.P. Hiernaut, M. Sheindlin, C. Ronchi, Fourth Euro Ceramics 3 (1995) 3.
[29] C. Ronchi, J.P. Hiernaut, J. Alloys Compd. 240 (1996) 179.
[30] M.T. Hutchings, J. Chem. Soc., Faraday Trans. 2 (83) (1987) 1083.
[31] K. Clausen, W. Hayes, J. Emyr Macdonald, P. Schnabel, M.T. Hutchings, J.K. Kjems, High Temp. High Press. 15 (1983) 383.
[32] K. Clausen, W. Hayes, M.T. Hutchings, J.K. Kjens, J.E. Macdonald, R. Osborn, High Temp. Sci. 19 (1985) 189.
[33] M.T. Hutchings, K. Clausen, W. Hayes, J.E. Macdonald, R. Osborn, P. Schnabel, High Temp. Sci. 20 (1985) 97.
[34] B. Weidenbaum, H. Hausner, Trans. Amer. Nucl. Soc. 8 (1965) 32.
[35] L. Leibowitz, M.G. Chasanov, L.W. Mishler, D.F. Fischer, J. Nucl. Mater. 39 (1971) 115.
[36] R.K. Edwards, M.S. Chandrasekharaiah, P.M. Danielson, High Temp. Sci. 1 (1969) 98.
[37] J.A. Christensen, Report HW-69234, Hanford Atomic Products Operation Richland, Washington, 1962, 24 pp.
[38] M. Baïchi, Ph.D., Contribution à l'étude du corium d'un réacteur nucléaire accidenté: aspects puissance résiduelle et thermodynamique des systèmes U–UO_2 et UO_2–ZrO_2, Institut National Polytechnique de Grenoble, 24 Septembre 2001, Grenoble, France.
[39] M. Baïchi, C. Chatillon, G. Ducros, C. Guéneau, Congrès CNRS MATERIAUX2002, 21–25 Oct. 2002, Tours, France (CD available).
[40] J.L. Bates, J. Amer. Ceram. Soc. 49 (1966) 395.
[41] J.S. Anderson, J.O. Sawyer, H.W. Worner, G.M. Willis, M.J. Banmister, Nature 185 (1960) 915.
[42] J.D. Cox, D.D. Wagman, V.A. Medvedev, Codata key values for thermodynamics, Hemisphere Publishing Corporation, N.Y., 1989, p. 234.
[43] R.A. Hein, P.N. Flagella, J.B. Conway, J. Amer. Ceram. Soc. 51 (1968) 291.
[44] L. Leibowitz, L.W. Misher, M.G. Chasanov, J. Nucl. Mater. 29 (1969) 356.
[45] E.A. Aitken, H.C. Brassfield, R.E. Fryxell, in: Thermodynamics, Vol. II, Int. Atomic Energy Agency, Vienna, Austria, 1966, p. 435.
[46] C.A. Alexander, J.S. Ogden, G.W. Cumingham, Report No. BMI-1789, January 6, 1967, 26 pp.
[47] T.L. Markin, V.J. Wheeler, R.J. Bones, J. Inorg. Nucl. Chem. 30 (1968) 807.
[48] M. Tetenbaum, P.D. Hunt, J. Chem. Phys. 49 (1968) 4739.
[49] R. Szwarc, R.E. Latta, J. Amer. Ceram. Soc. 51 (1968) 264.
[50] V.J. Wheeler, J. Nucl. Mater. 39 (1971) 315.
[51] V.J. Wheeler, I.G. Jones, J. Nucl. Mater. 42 (1972) 117.
[52] N.A. Javed, J. Nucl. Mater. 43 (1972) 219.
[53] T.L. Markin, R.J. Bones, Report AERE-R4178, Nov. 1962, 41pp.
[54] V.G. Baranov, Yu.G. Godin, Atom. Energy (Translation) 51 (1981) 228.
[55] C. Thomas, P. Gerdanian, M. Dodé, J. Chim. Phys. Phys. Chim. Biol. 65 (1968) 1349.
[56] P. Gerdanian, M. Dodé, J. Chim. Phys. (1965) 171.
[57] A.J. Baker, PhD thesis, A transpiration apparatus for determining vapor pressures of metal oxides, Illinois Institute of Technology, 1971. Available at UMI Dissertation Services, 300 Noth Zeeb Road, P.O. Box 1346, Ann Arbor, MI 48106-1346, USA.

[58] R.J. Ackermann, E.G. Rauh, M.S. Chandrasekharaiah, J. Phys. Chem. 73 (1969) 762 (see also Report ANRL-7048, July 1965, 34 pp).
[59] A. Pattoret, Ph.D., Etudes Thermodynamiques par Spectrométrie de masse sur les systèmes uranium-oxygen et uranium-carbone, Université Libre de Bruxelles, 20 mai 1960, Belgique (Available from Universities Inter library Services).
[60] A. Pattoret, J. Drowart, S. Smoes, in: Thermodynamics of Nuclear Materials, Int. Atomic Energy Agency, Vienna, 1968, p. 613.
[61] J. Drowart, A. Pattoret, S. Smoes, in: Proceedings of the Bristish Ceramic Society, Vol. 8, 1967, p. 67.
[62] A. Pattoret, J. Drowart, S. Smoes, Bull. Soc. Française de Céramique 77 (1967) 76.
[63] E.K. Storms, J. Nucl. Mater. 132 (1985) 231.
[64] M. Baïchi, C. Chatillon, C. Guéneau, J. le Ny, J. Nucl. Mater. 303 (2002) 196.
[65] E.A. Schaefer, M.R. Menke, J.O. Hibbits, Report No. GE-TM 66-4-9, 1966.
[66] A.J. Chapman, R.E. Meadows, J. Amer. Ceram. Soc. 47 (1964) 614.
[67] P.E. Blackbourn, J. Phys. Chem. 62 (1958) 897.
[68] R.J. Ackermann, A.T. Chang, J. Chem. Thermodyn. 5 (1973) 873.
[69] M.W. Chase Jr., NIST-JANAF Thermochemical Tables, fourth ed., 1998, J. Phys. Chem. Ref. Data., Monograph 9, Nat. Inst. Standards Technology, Gaithersburg, MD 20889-0001, USA.
[70] F. Defoort, C. Chatillon, Report CEA-R-6027, 2003, CEA/SACLAY91191, Gif-sur-Yvette cedex, France (in English).
[71] C. Chatillon, M. Allibert, A. Pattoret, in: The Characterization of high temperature vapors and gases, N.B.S. Special Pub. 561, 1978.
[72] J. Drowart, C. Chatillon, J. Hastie, D. Bonnell, High Temperature Mass Spectrometry: Instrumental Techniques, Ionization Cross-Sections, Pressure Measurements and Thermodynamic Data, Pure Appl. Chem. 77 (2005) 683.
[73] C. Younés, Ph.D. at Université de Paris-Sud, Orsay, France, Order 14-3199, 26 June 1986.
[74] G. de Maria, R.P. Burns, J. Drowart, M.G. Inghram, J. Chem. Phys. 32 (1960) 1373.
[75] C. Chatillon, M. Allibert, A. Pattoret, High Temp. Sci. 8 (1976) 233.
[76] N.L. Winterbottom, J. Chem. Phys. 47 (1967) 3546.
[77] C. Chatillon, A. Pattoret, J. Drowart, High Temp. High Press. 7 (1975) 119.
[78] C. Chatillon, Electrochem. Soc. Proc. 97 (1997) 648.
[79] C. Chatillon, La Revue de métallurgie – CIT/Science et Génie des Matériaux, 1998, p. 1077.
[80] P. Morland, C. Chatillon, P. Rocabois, High Temp. Mater. Sci. 37 (1997) 167.
[81] R.J. Ackermann, E.G. Rauh, M.H. Rand, A re-determination and re-assessment of the thermodynamics of sublimation of uranium dioxide, in: 5th International Symposium on Thermodynamics of Nuclear Materials, 29 January–2 February 1979, AIEA, Jülich, Germany. Thermodynamics of Nuclear Materials, 1979, vol. 1, IAEA Vienna, 1980, p. 11.
[82] E. Kato, J. Mass Spectrom. Soc. Jpn. 41 (1993) 297.
[83] E.K. Storms, B.A. Mueller, Nat. Bur. Standards (presently NIST, see Ref. [64]), Special Pub. 561, in: Proceedings of 10th Mater. Res. Symp. on characterization of High Temp. Vapors and Gases, 1978, p. 143.
[84] P. Gerdanian, M. Dodé, in: Thermodynamics of Nuclear Materials, IAEA, Vienna, 1967, p. 41.
[85] P. Gerdanian, Colloque CNRS, Thermochimie, Marseille, France, 1971, p. 1.
[86] B. Lindemer, T.M. Besmann, J. Nucl. Mater. 130 (1985) 473.
[87] C. Guéneau, M. Baïchi, D. Labroche, C. Chatillon, B. Sundman, J. Nucl. Mater. 304 (2002) 161.
[88] P.Y. Chevalier, E. Fischer, B. Cheynet, J. Nucl. Mater. 303 (2002) 1.